

DRAFT DISCLAIMER

This contractor document was prepared for the U.S. Department of Energy (DOE), but has not undergone programmatic, policy, or publication review, and is provided for information only. The document provides preliminary information that may change based on new information or analysis, and is not intended for publication or wide distribution; it is a lower level contractor document that may or may not directly contribute to a published DOE report. Although this document has undergone technical reviews at the contractor organization, it has not undergone a DOE policy review. Therefore, the views and opinions of authors expressed do not necessarily state or reflect those of the DOE. However, in the interest of the rapid transfer of information, we are providing this document for your information, per your request.

**OFFICE OF CIVILIAN RADIOACTIVE WASTE MANAGEMENT
ANALYSIS/MODEL COVER SHEET**

1. OA: QA

Page: 1 of 67

Complete Only Applicable Items

<p>2. Analysis Check all that apply</p> <table border="1" style="width:100%; border-collapse: collapse;"> <tr> <td style="width:20%;">Type of Analysis</td> <td> <input type="checkbox"/> Engineering <input type="checkbox"/> Performance Assessment <input checked="" type="checkbox"/> Scientific </td> </tr> <tr> <td>Intended Use of Analysis</td> <td> <input type="checkbox"/> Input to Calculation <input checked="" type="checkbox"/> Input to another Analysis or Model <input type="checkbox"/> Input to Technical Document </td> </tr> <tr> <td colspan="2">Describe use: Support for Waste Form PMR</td> </tr> <tr> <td colspan="2"> </td> </tr> <tr> <td colspan="2"> </td> </tr> </table>	Type of Analysis	<input type="checkbox"/> Engineering <input type="checkbox"/> Performance Assessment <input checked="" type="checkbox"/> Scientific	Intended Use of Analysis	<input type="checkbox"/> Input to Calculation <input checked="" type="checkbox"/> Input to another Analysis or Model <input type="checkbox"/> Input to Technical Document	Describe use: Support for Waste Form PMR						<p>3. Model Check all that apply</p> <table border="1" style="width:100%; border-collapse: collapse;"> <tr> <td style="width:20%;">Type of Model</td> <td> <input type="checkbox"/> Conceptual Model <input type="checkbox"/> Abstraction Model <input type="checkbox"/> Mathematical Model <input type="checkbox"/> System Model <input type="checkbox"/> Process Model </td> </tr> <tr> <td>Intended Use of Model</td> <td> <input type="checkbox"/> Input to Calculation <input type="checkbox"/> Input to another Model or Analysis <input type="checkbox"/> Input to Technical Document </td> </tr> <tr> <td colspan="2">Describe use:</td> </tr> <tr> <td colspan="2"> </td> </tr> <tr> <td colspan="2"> </td> </tr> </table>	Type of Model	<input type="checkbox"/> Conceptual Model <input type="checkbox"/> Abstraction Model <input type="checkbox"/> Mathematical Model <input type="checkbox"/> System Model <input type="checkbox"/> Process Model	Intended Use of Model	<input type="checkbox"/> Input to Calculation <input type="checkbox"/> Input to another Model or Analysis <input type="checkbox"/> Input to Technical Document	Describe use:					
Type of Analysis	<input type="checkbox"/> Engineering <input type="checkbox"/> Performance Assessment <input checked="" type="checkbox"/> Scientific																				
Intended Use of Analysis	<input type="checkbox"/> Input to Calculation <input checked="" type="checkbox"/> Input to another Analysis or Model <input type="checkbox"/> Input to Technical Document																				
Describe use: Support for Waste Form PMR																					
Type of Model	<input type="checkbox"/> Conceptual Model <input type="checkbox"/> Abstraction Model <input type="checkbox"/> Mathematical Model <input type="checkbox"/> System Model <input type="checkbox"/> Process Model																				
Intended Use of Model	<input type="checkbox"/> Input to Calculation <input type="checkbox"/> Input to another Model or Analysis <input type="checkbox"/> Input to Technical Document																				
Describe use:																					

4. Title:
Colloid-Associated Radionuclide Concentration Limits; ANL

5. Document Identifier (including Rev. No. and Change No., if applicable):
ANL-EBS-MD-000020 REV 00

6. Total Attachments: N/A	7. Attachment Numbers - No. of Pages in Each: N/A
-------------------------------------	---

	Printed Name	Signature	Date
8. Originator	Carol J. Mertz	<i>Carol J. Mertz</i>	2/16/00
9. Checker	Steve Kung	<i>Stephen Kung</i>	3-16-2000
10. Lead/Supervisor	Christina Stockman	<i>Christina Stockman</i>	3-16-2000
11. Responsible Manager	David Stahl	<i>H.E. Stahl for</i>	3-16-2000

12. Remarks:

**PRELIMINARY DRAFT
INFORMATION ONLY**

**INFORMATION COPY
LAS VEGAS DOCUMENT CONTROL**

DF03

**OFFICE OF CIVILIAN RADIOACTIVE WASTE
MANAGEMENT
ANALYSIS/MODEL REVISION RECORD**
Complete Only Applicable Items

1. Page: 2 of 57

2. Analysis or Model Title:

Colloid-Associated Radionuclide Concentration Limits: ANL

3. Document Identifier (including Rev. No. and Change No., if applicable):

ANL-EBS-MD-000020 REV 00

4. Revision/Change No.

5. Description of Revision/Change

REV 00

Initial Issue

CONTENTS

	Page
ACRONYMS AND ABBREVIATIONS	7
1. PURPOSE	8
2. QUALITY ASSURANCE	8
3. COMPUTER SOFTWARE AND MODEL USAGE	8
4. INPUTS.....	9
4.1 DATA AND PARAMETERS	9
4.2 CRITERIA	9
4.3 CODES AND STANDARDS.....	10
5. ASSUMPTIONS	10
6. ANALYSIS/MODEL.....	11
6.1 INTRODUCTION	11
6.2 THE NATURE OF WASTE FORM COLLOIDS	13
6.2.1 Properties of Colloids Generated from Glass Tests.....	14
6.2.2 Colloids Generated from Spent Fuel Corrosion	30
6.3 SIZE DISTRIBUTION OF WASTE FORM COLLOIDS.....	35
6.3.1 Size Distribution of Colloids Generated from Glass Corrosion	36
6.3.2 Size Distribution of Colloids Generated from Spent Fuel Corrosion.....	40
6.4 QUANTIFICATION OF WASTE FORM COLLOIDS	43
6.4.1 Quantification of Colloids Generated from Glass Tests.....	43
6.4.2 Recommendations for Modeling Colloid Generation.....	44
6.4.3 Quantification of Colloids Generated from Spent Fuel Corrosion.....	49
7. CONCLUSIONS.....	50
8. INPUTS AND REFERENCES	52
8.1 DOCUMENTS CITED.....	52
8.2 CODES, STANDARDS, REGULATIONS, AND PROCEDURES.....	55

FIGURES

	Page
Figure 1. Types of Radionuclide-Bearing Colloids.....	11
Figure 2. Schematic of Colloid Formation from Waste Form.....	13
Figure 3. TEM Micrograph of a Smectite Clay Colloid Bearing Substantial Uranium from the 70-Day Corrosion Test of SRL 131A with EJ-13 at 2,000 m ⁻¹ and 90°C.....	16
Figure 4. The EDS Spectrum Obtained from the Uranium-Rich Smectite Clay Particle in Figure 3	16
Figure 5. Total Silica in Solution (colloidal and dissolved) as a Function of Test Duration for Static Corrosion Tests on SRL 202A, SRL 202U, and SRL 131A Glasses.....	18
Figure 6. Sum of Al, Fe, and Mg Concentrations as a Function of Total Silica in Solution (Colloidal and Dissolved) for Static Corrosion Tests on SRL 202A, SRL 202U and SRL 131A at Various S/V (T = 90°).....	20
Figure 7. Ionic Strength as a Function of Glass Corrosion for SRL 202A and SRL 131A at 2,000 and 20,000/m (T = 90°C).....	21
Figure 8. Plutonium Concentration from Plutonium-Bearing Colloids as a Function of Ionic Strength for Corrosion Tests on SRL 202A and SRL 131A at 2,000 and 20,000/m (at 90°C).....	22
Figure 9. The Clay Layer on Glass after 38 Weeks of Testing in the N3 Series.....	23
Figure 10. The Cumulative Normalized Release of the Elements B, Np, Pu, and Am from One of the Tests in the N2 Series.....	24
Figure 11. Transmission Electron Microscopy Micrograph of Clay Colloid Particles Extracted from the Glass Drip Tests.....	25
Figure 12. Smectite Clay Colloids from the N3 Glass Drip Tests with Entrained Particles of Brockite (dark regions within clay matrix).....	26
Figure 13. TEM Image and EELS Analysis of a REE-Bearing Phase from a 200R Glass Drip Test (N4)	26
Figure 14. The N3-10 Glass Monolith after about 8 Years of Testing.....	27
Figure 15. The Clay Alteration Layer on the N3-10 Glass after approximately 8 Years of Testing.....	28
Figure 16. EDS Spectra of the Three Components Comprising the N3-10 Clay Composite.....	29
Figure 17. The EELS Spectra from the Brockite Particles.....	29
Figure 18. Bright-Field TEM Image of Particles from 57 Day Sampling from an ATM-103 Test.....	31
Figure 19. Electron Energy-Loss Spectroscopy of Colloid from S32J-57.....	32
Figure 20. (a) Example of Smectite Clay Colloids from Corrosion Test with ATM-106 and (b) X-ray Energy Dispersive Analysis of Clay Colloid from an ATM-103 Test.....	33
Figure 21. (a) Transmission Electron Microscopy Image of Pu-Rich Regions within the Corroded ATM-106 Fuel Reacted under High-Drip-Rate Conditions for 5 Years and (b) Compositional Analysis of the Fuel and Altered Regions.....	34
Figure 22. Amount of Plutonium and Americium Released from SRL 202A Static Corrosion Tests at 2,000/m (T = 90°C).....	38
Figure 23. Mean Diameter of Waste Form Colloids Generated from the Corrosion of the SRL 131A Glass in EJ-13 at 2,000/m (T = 90°C) as a Function of Test Duration.....	39

FIGURES (Continued)

	Page
Figure 24. Concentration of Pu Colloids and Total Colloid Concentration as a Function of Test Duration for the SRL 131A Glass at 2,000/m (T = 90°C)	40
Figure 25. The Pu Distribution in the Leachate as a Function of Time from High-Drip-Rate Tests on the ATM-103 and ATM-106 Fuels.....	41
Figure 26. Particle Distribution for Colloids in Leachate from 56 Month ATM-106 Vapor Test.....	42
Figure 27. Ratio of Normalized Mass Loss of Plutonium to Normalized Mass Loss of Boron as a Function of Test Duration (in days) for Static Corrosion Tests on the SRL 202A and SRL 131A Glasses.....	44
Figure 28. Normalized Release Rate of Colloidal Plutonium as a Function of Normalized Mass Loss of Boron for SRL 202A and SRL 131A Glasses at 2,000 and 20,000/m..	45
Figure 29. Plutonium Release Rate versus Cumulative Boron Release for N2 and N3 Glass-Drip Tests	46
Figure 30. The Fractional Release Rate of Pu as a Function of Cumulative Fractional Tc Release for the ATM-103 and ATM-106 High-Drip-Rate Tests.....	49

TABLES

	Page
Table 1. Data Inputs Used in the Analysis Development.....	9
Table 2. Assumptions Used in the Analysis Development.....	10
Table 3. Filtrate Concentrations from Filtration through 450 and 6 nm Filters on Leachates from Corrosion Tests with SRL 202U in EJ-13 (20,000/m and 90°C).....	17
Table 4. Silica Concentration and Mass of Plutonium in Dissolved and Colloidal Fractions of the Leachate from Static Corrosion Tests on the SRL 202A and SRL 131A at Various Surface Area of Glass to Solution Volume Ratios (T = 90°C).....	19
Table 5. Percentage of Plutonium and Americium Released as Colloidal (c), Dissolved (d), and Adsorbed (a) Forms in Leachates of Corrosion Tests with SRL 202A and SRL 131A at 2,000 and 20,000/m.....	37

ACRONYMS AND ABBREVIATIONS

AEM	analytical electron microscopy
AMR	Analysis/Model Report
ANL	Argonne National Laboratory
CSNF	commercial spent nuclear fuel
CRWMS	Civilian Radioactive Waste Management System
DIRS	Document Input Reference System
DIW	deionized water
DLS	dynamic light scattering
DOE	U.S. Department of Energy
DWPF	Defense Waste Processing Facility
EDS	energy dispersive x-ray spectroscopy
EELS	electron energy loss spectroscopy
HLW	high-level waste
ICP-MS	inductively coupled plasma-mass spectrometry
M&O	Management and Operating Contractor
NL	normalized mass loss
NR	normalized rate
OTED	oblique textured electron diffraction
PMR	Process Model Report
REE	rare earth elements
SAED	selected area electron diffraction
SRL	Savannah River Laboratory
TEM	transmission electron microscopy
WVDP	West Valley Demonstration Project
YMP	Yucca Mountain Site Characterization Project

1. PURPOSE

The purpose and scope of this report is to describe the analysis of available colloidal data from waste form corrosion tests at Argonne National Laboratory (ANL) to extract characteristics of these colloids that can be used in modeling their contribution to the source term for sparingly soluble radioelements (e.g., Pu). Specifically, the focus is on developing a useful description of the following waste form colloid characteristics: (1) composition, (2) size distribution, and (3) quantification of the rate of waste form colloid generation. The composition and size distribution information are intended to support analysis of the potential transport of the sparingly soluble radionuclides associated with the waste form colloids. The rate of colloid generation is intended to support analysis of the waste form colloid-associated radionuclide concentrations. In addressing the above characteristics, available data are interpreted to address mechanisms controlling colloid formation and stability.

This report was developed in accordance with the *Development Plan for Waste Package Materials Department Analysis and Modeling Reports Supporting the Waste Form PMR* (CRWMS M&O 2000). It specifically addresses the item, "Colloid-Associated Radionuclide Concentration Limits: ANL" of the product development plan and is in compliance with procedure AP3.10Q.

Because the end objective is to support the source term modeling we have organized the conclusions into two categories: (1) data analysis conclusions and (2) recommendations for colloid source term modeling. The second category is included to facilitate use of the conclusions from the data analysis in the abstraction of a colloid source term model.

The data analyses and conclusions that are presented in this report are based on small-scale laboratory tests conducted on a limited number of waste glass compositions and spent fuel types.

2. QUALITY ASSURANCE

The Quality Assurance (QA) program applies to this analysis. All types of waste packages were classified (per QAP-2-3) as Quality Level-1. This analysis applies to all of the waste package designs included in the Monitored Geologic Repository (MGR) Classification Analyses. Reference CRWMS M&O (1999a), *Classification of the MGR Uncanistered Spent Nuclear Fuel Disposal Container System*, is cited as an example. The development of this analysis is conducted under activity evaluation *1101213FM3 Waste Form Analyses & Models - PMR* (CRWMS M&O 1999b) which was prepared per QAP-2-0. The results of that evaluation were that the activity is subject to the *Quality Assurance Requirements and Description* (DOE 2000) requirements.

3. COMPUTER SOFTWARE AND MODEL USAGE

No software was used to support the analysis. Macintosh Operating System 8.5.1 was used during analysis of the data in this document. Commercial software (Excel 98 and Kaleidagraph, version 3.0) was used to compile test data and plot results using standard functions. The originator and checker verified the plots against the original data. No user defined routines were implemented.

4. INPUTS

4.1 DATA AND PARAMETERS

Technical product inputs are listed Table 1 and on the Document Input Reference System (DIRS) as stipulated by AP-3.10Q. Data used in this AMR are not directly used in producing a technical product that provides any estimates for any of the principal factors or potentially disruptive events and processes and is thus labeled qualified verification level 2.

Table 1. Data Inputs Used in the Analysis Development

Parameter	Description
LL991001251021.090	Draft - CSNF Waste Form Degradation: Unsaturated Drip Tests - G2020 Analysis and Modeling Report
LL000122051021.116	Plutonium and americium concentrations in various size fractions in the corrosion leachates of the SRL 131A and SRL 202A glasses at surface area to volume ratios of 2,000 and 20,000/m
LL000123351021.117	Cation concentrations and pH values for corrosion leachates of the SRL 131A, SRL 202A, and SRL 202U glasses at various surface area to volume ratios
LL991110751021.104	Transmission electron microscopy (TEM) micrograph of spallation of clay alteration phase from glass drip tests
LL991110251021.099	Summary of TEM analyses from glass corrosion tests indicates that clay colloids are the major phase and clay colloids are observed in the spent fuel tests. TEM analyses (micrograph, EELS spectrum) of spent fuel particles and rare earth element- (REE) rich colloids.
LL991110851021.105	TEM analyses of spent fuel colloids from ATM-106 low drip rate test
LL991110651021.103	TEM analysis (micrograph) of clay layer on surface of glass from N3 drip tests
LL991110051021.097	TEM analyses (micrograph, EDS spectrum) of smectite clay colloids from spent fuel tests
LL991109951021.096	TEM analyses (micrographs, EELS spectra) of colloids that are composed of a REE-bearing phase or a transuranic-bearing brockite phase from glass drip tests
LL991110451021.101	TEM analyses (micrographs, EDS and EELS spectra) of clay colloids from glass drip tests
LL991109851021.095	DLS analyses of leachates from spent fuel corrosion tests
LL991110351021.100	TEM analyses (micrograph and EDS spectrum) of Pu-rich regions in reacted ATM-106 fuel.
LL991109751021.094	Analyses of corrosion leachates from SRL 131A, 202A, and 202U glasses at various surface area to volume ratios
LL000205551021.118	Plutonium and boron release data from N2 and N3 drip tests (data used to generate Figure 29)
LL991110551021.102	Discussion of colloid generation model and analysis of plutonium and boron release data from glass drip tests

4.2 CRITERIA

The analyses developed in this Analysis/Model Report (AMR) are not based upon design or other criteria.

4.3 CODES AND STANDARDS

No codes or standards are used in this AMR.

5. ASSUMPTIONS

Assumptions made to perform the analyses in this document are presented in Table 2 and are incorporated into the discussion in Section 6 of this document.

Table 2. Assumptions Used in the Analysis Development

Assumption	Basis	Section Used
The measured waste form colloid characteristics (composition, size distribution, and rate of generation) are determined by the waste form and not the testing setup. Specifically, it was assumed that sorption of colloids onto the test vessel walls didn't effect the rate of colloid generation and that the sample holder configuration in the spent fuel (SF) tests does not effect the release of filterable material.	Consistent data from numerous glass tests and conservative estimates are provided for the colloidal Pu release. However, for the SF tests, effects of filtration due to sample holder configuration are not known. For this reason, a conservative bounding estimate (see Fig. 30) was used to estimate the rate of Pu colloid generation.	6
The TEM phase identification techniques provide data that are representative of waste form colloids.	Justified by multiple analyses and experience of analyst.	6
The filterable material (obtained from sequential filtration) is colloidal or particulate.	Data from complementary techniques gives consistent results (see Fig. 24).	6.2.1, 6.3, 6.4
Dynamic light scattering (DLS) provides an accurate representation of the size distribution of the waste form colloids.	Data from filtration technique gives results consistent with DLS (see Fig. 24).	6.3
Ionic strength can be calculated from the major cations in solution.	Other species are present at much lower concentrations and would not contribute significantly to the ionic strength.	6.2.1
The normalized mass loss of B and Tc indicate the extent of glass and spent fuel corrosion, respectively.	B is accepted for glass corrosion. Boron is used as a marker of the extent of glass corrosion since it a highly soluble glass component, and it does not get incorporated into alteration phases. Tc is believed to be the best indicator for SF. Technetium is a soluble element, which is released from the fuel to a greater extent than other elements, such as Cs and Sr (these are incorporated in alteration phases).	6.4

The effect of the sample holder configuration on the release of Pu in the SF tests is not known and, therefore, the estimated bounding rate of Pu colloid generation based on the test data (Fig. 30) needs further confirmation. If greater confidence is required (e.g., if TSPA calculations

show that the waste form colloids can contribute significantly to the overall system performance), then confirmatory testing will be performed per the guidelines of ASTM (1997).

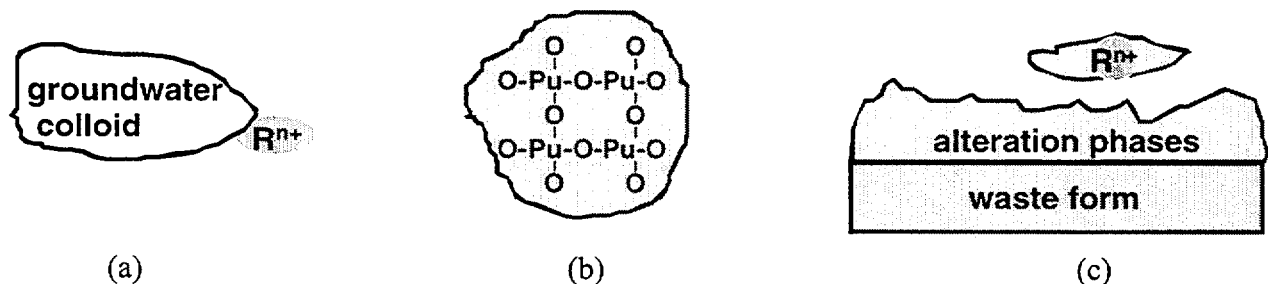
6. ANALYSIS/MODEL

This section provides the analyses and the theoretical understanding to support the following waste form colloid characteristics: (1) composition, (2) size distribution, and (3) quantification of the rate of waste form colloid generation.

6.1 INTRODUCTION

Colloids have the potential to transport radioactive contaminants from a waste storage or disposal site. Recent studies at the Nevada Test Site have shown the mobility of plutonium to be associated with colloids composed of clays, zeolites, and cristobalite (Kersting et al. 1999). In order to understand the transport of colloids, it is necessary to characterize the physical and chemical nature of the solution-borne colloids that form during degradation of the waste forms, specifically as related to actinide releases. The results presented in this report provide a basis for modeling waste form colloid-associated radionuclide concentrations.

Colloidal systems encompass a wide variety of surface active agents and dispersed particles, typically with one dimension in the size range of 1 nm to 1 μm . The radionuclide-bearing colloids that are generated from the corrosion of commercial spent nuclear fuel and high level waste glass are the focus of this report. Several types of radionuclide-bearing colloids may be formed during the corrosion of the waste form: real, pseudo, and waste form colloids (Fig. 1).



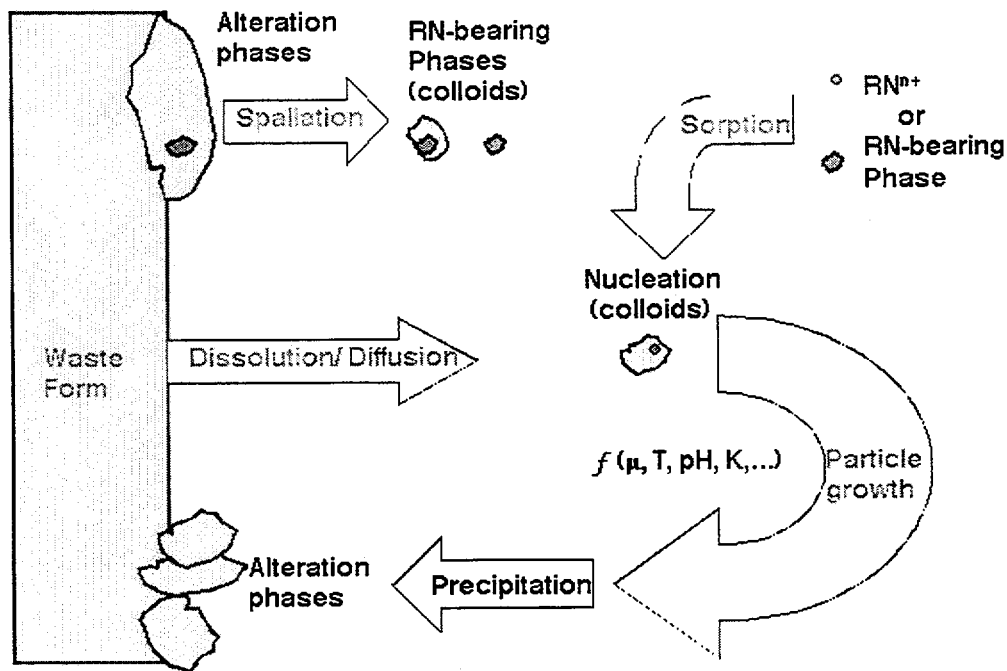
NOTE: Several types of radionuclide-bearing colloids are depicted: (a) pseudo-colloids, (b) real colloids, and (c) waste form colloids. The radionuclide (R^{n+}) associated with the pseudo and waste form colloids can be an ionic species, a real colloid, or a discrete radionuclide-bearing phase. The size range for the colloids is 1 to 1,000 nm.

Figure 1. Types of Radionuclide-Bearing Colloids

Real colloids are formed from the hydrolysis and polymerization of actinide ions dissolved in solution. The rate of hydrolysis depends on the oxidation state of the ion. Actinide (An) ions tend to hydrolyze in the following order: $An^{4+} > AnO_2^{2+} > An^{3+} > AnO_2^+$ (Kim 1994). The formation of real colloids will be solubility limited based on the solution chemistry and prevents significant introduction of the real colloids to the environment. The incorporation, adsorption, or ion-exchange of radionuclides onto pre-existing groundwater colloids allows the transport of radionuclides via pseudo colloids. These pseudo colloids can increase the apparent solubility of actinides in solution and may enhance migration in aquifer systems. Transport of radionuclide contaminants at numerous waste sites have been underestimated by models when compared to

the field data where measurable concentrations of radionuclides have been detected migrating as colloids from the waste (McCarthy and Degueldre 1993). Most importantly, waste form corrosion can lead to the formation of another type of colloid known as primary or waste form colloids (Buck and Bates 1999; Finn et al. 1994a; Fortner et al.1997a). The formation of such colloids may allow actinide concentrations in solution that are significantly higher than achievable with real or pseudo colloids. The characterization of the physical and chemical nature of colloids is essential for understanding phenomena related to colloid stability, association, and adsorption properties. The contaminant oxidation state and solution chemistry are major factors. Other factors that determine the introduction of a contaminant to the environment are geology, hydrochemistry, and waste form composition. Release of the contaminant depends on complex geochemical equilibria (McCarthy and Degueldre 1993). Radionuclides released from waste glass or spent fuel may form real colloids, pseudo colloids, or primary colloids. The properties governing the stability of dispersed colloids are sensitive to the environment (pH, temperature, solution components).

Colloids are known to form by a variety of processes, which include condensation and dispersion (Ahn et al. 1993; Geckeis et al. 1998; McCarthy and Degueldre 1993). The condensation processes involve nucleation and growth of the colloid from a saturated solution. Colloids formed from dispersion processes involve subdivision, or spallation (fragmentation) of bulk material. Figure 2 represents the processes governing the formation of colloids during the corrosion of the waste form.



NOTE: Schematic of colloid formation from waste form corrosion wherein several processes are represented: (1) Spallation of radionuclide (RN) bearing alteration phases from the waste form that are within the colloidal size range and (2) Nucleation of colloids from dissolution of waste form and sorption of ionic RN species or RN-bearing phases. Particle growth is controlled by factors such as ionic strength, temperature, pH, solubility, and others. When particle diameters exceed colloidal dimensions (gravitational forces become dominant) or solution chemistry destabilizes the colloids, precipitation of RN-bearing alteration phases occurs.

Figure 2. Schematic of Colloid Formation from Waste Form

6.2 THE NATURE OF WASTE FORM COLLOIDS

The analyses presented in this section summarize the composition and properties of colloids generated during the corrosion of defense high level waste glass and commercial spent nuclear fuel. Data used in these analyses include at least ten years of testing for the static glass tests (Ebert 1995; Buck and Bates 1999; DTN: LL991110251021.099), over ten years of testing for the glass drip tests (Fortner and Bates 1996; Fortner et al. 1997a, 1997b; DTN: LL000205551021.118), and over four years of testing for the spent fuel tests (Finn et al. 1994a, 1994b; LL991001251021.090). The methods employed for colloid characterization in this section are TEM and filtration (analysis of filtrates with inductively coupled plasma-mass spectrometry (ICP-MS) or alpha spectroscopy). In summary, smectite clay colloids that are formed during glass corrosion contain discrete radionuclide-bearing phases incorporated in the clay. The stability of these colloids is governed by the properties of the clay and the geochemical environment.

TEM is an excellent method for determining morphology, structure, and elemental composition (by energy dispersive x-ray spectroscopy [EDS], electron diffraction [ED], and electron energy loss spectroscopy [EELS]) of small, electron transparent particles. However, owing to the small sample size employed in the sample preparation, the particles isolated and examined may not be representative of the colloid population because of the very small sample sizes. In addition, sample preparation may result in artifacts, which may effect the particle size determined with TEM. Numerous TEM samples and complementary analyses from other colloid characterization techniques (filtration and dynamic light scattering [DLS]) are used to increase our confidence in the observed results. In an effort to quantify the uncertainties with TEM, McCarthy and Degueldre (1993) report estimates required for microscopic investigations of colloids. For 100 nm colloids and a leachate volume of 2 and 20 μL , a concentration of 2×10^{13} and 2×10^{12} particles/L, respectively, corresponds to the optimal detection of colloids (5% coverage of a 3 mm diameter and 7 mm^2 surface area TEM grid). This concentration decreases by an order of magnitude for 10 nm colloids at both sample volumes. Our experiments used a leachate volume of 5 μL , between the 2 and 20 μL volume used by McCarthy and Degueldre (1993); thus, their estimates of colloid populations for optimal detection of colloids from microscopic investigations give a range of optimal detection for our TEM samples.

Sequential filtration is one technique used to separate various colloids from each other and to determine the extent of contaminant association with the colloids. In the procedure, the solution is filtered successively through a series of membranes of decreasing pore size with the filtrate of one step being filtered through the following membrane. Aliquots of the filtrates are submitted for chemical analysis. The elemental composition and activity of radionuclides associated with a colloidal size fraction are determined using inductively coupled plasma-mass spectrometry and by nuclear spectroscopy, respectively. Filtration is one technique used to separate particles of various sizes with minimum perturbation. While filtration is a good technique for determining the size partitioning of actinide-bearing colloids, it is important to recognize some potential artifacts (e.g., retention of particles smaller than the pore size due to interaction with the filter membrane). Colloids larger than the nominal pore size of the filter are assumed to be totally retained, and smaller colloids are assumed to pass through the filter. Results from filtration also assume that no reactions (electrostatic or chemical interactions) occur between the colloid and the filter material (McCarthy and Degueldre 1993, p. 288). However, confidence in the filtration data is gained from supporting data using other techniques.

6.2.1 Properties of Colloids Generated from Glass Tests

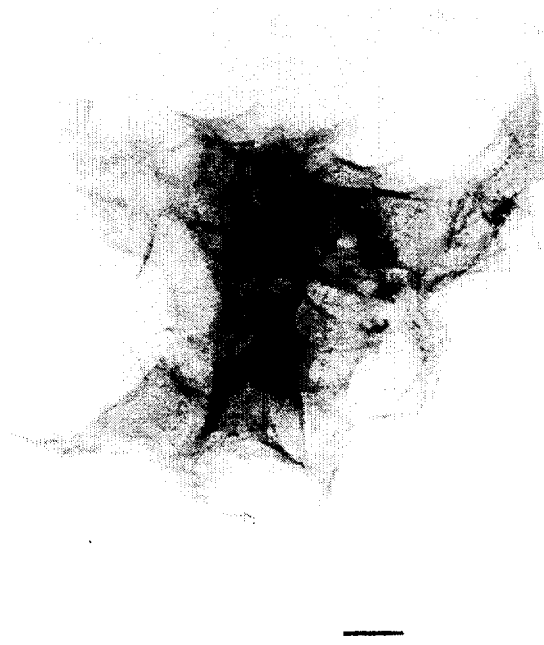
This section will focus on the composition, stability, and formation of colloidal species generated during static corrosion and long-term intermittent drip tests on radioactive waste glasses. During glass corrosion, smectite clay colloids are known to form, which contain discrete radionuclide-bearing phases. The transport of such radionuclide-associated colloids represents a potential source of mobile radionuclides.

Analyses will be presented in this section from static corrosion tests that were performed on several Defense Waste Processing Facility (DWPF) glass compositions at various surface area of glass-to-leachate volume ratios. A summary of the test results and a detailed description of the test procedure and glass compositions is found elsewhere (Ebert and Bates 1993, Ebert 1995). The types of glasses used in the tests were Savannah River Laboratory (SRL) 202A (actinide

doped), 202U (no actinides except uranium), and 131A (actinide doped). The glasses were used as a crushed powder (-100+200 mesh) or as monoliths with a 1 cm diameter and 1 mm width. Tests on the glasses were performed in equilibrated J-13 groundwater (EJ-13) or deionized water (DIW) in 304L stainless steel Parr vessels.

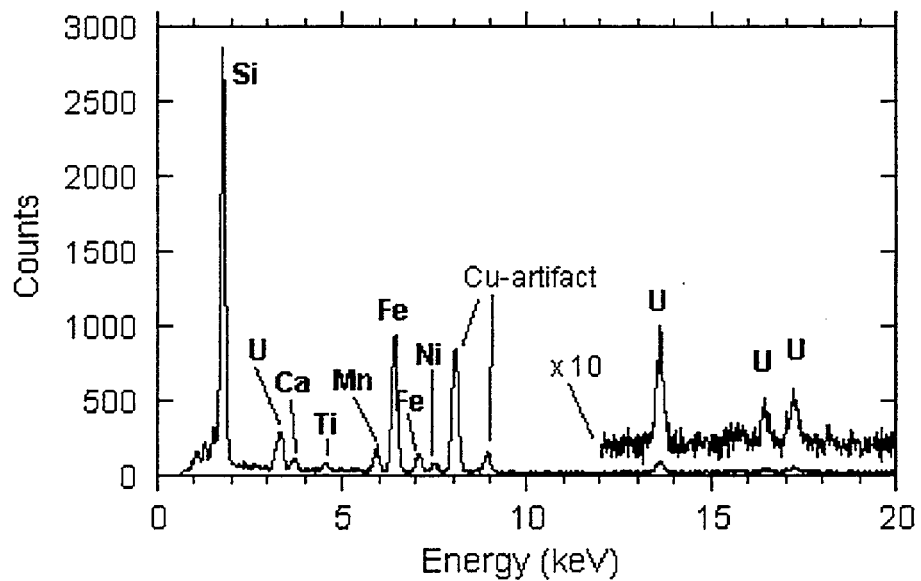
In the drip tests, 0.075 mL (about 3 drops) of groundwater from the J-13 well near Yucca Mountain, which had been equilibrated with Topopah Springs tuff (and is termed EJ-13 water) is injected onto the test assemblage in a sealed stainless steel test vessel every 3.5 days. Additional air is also injected into the test vessel with the water. Details of the test procedure are given elsewhere (Fortner et al. 1997a). Tests using actinide- and technetium-doped SRL 165 glass have been ongoing for over 12 years and are termed the N2 Tests. Tests with a West Valley Demonstration Project (WVDP) former reference glass (ATM-10) have been in progress for 10 years, and are referred to as the N3 Tests. Modified drip test with a radioactive sludge-based SRL 200R glass that had been pre-aged, along with its 304L stainless steel holder, in 200°C water vapor is termed the N4 Test and has been ongoing for over 7 years. Measurements and analyses from the N2 and N3 tests were reported in a February 1999 Data Package (DTN: LL000205551021.118).

Clay colloids are the major colloid phase observed in the static and drip glass tests (DTN: LL991110251021.099, pp. 156-157). Figure 3 provides an example of clay colloids formed during a static glass corrosion test. The morphology (Fig. 3) and EDS (Fig. 4) are consistent with a smectite clay. Other examples of clay colloids formed in the glass corrosion tests can be found in the following references: Bates et al. (1993, 1994, 1996); Bates and Buck (1994a, 1994b); Buck et al. (1993, 1994); Buck and Bates (1999); Cunnane and Bates (1991); and Feng et al. (1994). Clay colloids can be readily identified in the TEM, as they often produce oblique textured electron diffraction (OTED) patterns when tilted. OTED patterns result when clay crystallites settle onto the 'holey' carbon grid with c^* perpendicular to the 'holey' carbon support film. The resulting reciprocal lattice is a series of concentric circles lying on top of one another which, when tilted, result in the Ewald sphere passing through an ellipse (Feng et al. 1994). The small variations in the angle of the textured axis between clay colloids result in arcs rather than diffraction spots being produced. Buck et al. (1993) provides selected area diffraction patterns from textured clay colloids and the OTED pattern typical of a poorly crystalline smectite clay. The radionuclide-bearing phases are typically present as discrete phases that are associated with clay colloids. While the colloidal properties of the radionuclide-bearing phases embedded in the clay colloid matrix will be governed by the clay, information is needed on the chemical and physical properties of the enriched radionuclide-bearing phases which will effect the disassociation/association properties with the clay during transport in a repository environment. Clay colloids have also been observed during the corrosion of other waste glasses under static corrosion tests (Geckeis et al. 1998).



NOTE: The scale bar is 50 nm. Careful examination of the micrograph reveals possible microcrystals distinct from the clay that may be responsible for the excess uranium in this colloid (DTN: LL991110451021.101, p. 185).

Figure 3. TEM Micrograph of a Smectite Clay Colloid Bearing Substantial Uranium from the 70-Day Corrosion Test of SRL 131A with EJ-13 at 2,000 m⁻¹ and 90°C.



NOTE: DTN: LL991110451021.101 (p. 185)

Figure 4. The EDS Spectrum Obtained from the Uranium-Rich Smectite Clay Particle in Figure 3

Bulk solution analyses with ICP-MS of the filtrate fractions (<6 and <450 nm) from glass corrosion tests provide quantitative elemental compositions of the bulk solution colloids. The 450 nm filtrate contains colloidal and dissolved species, while the 6 nm filtrate has only

dissolved components. Table 3 is a summary of the SRL 202U leachate composition using ICP-MS (DTN: LL000123351021.117, pp. 254-259) from 450 and 6 nm filters for Al, Fe, Si, and B concentrations and pH values (average values were calculated when available from duplicate tests). The B concentration in both the 450 and 6 nm filtrates did not change significantly, which indicates that this component is dissolved. However, filtration of the leachate solution through the 6 nm filter removed most of the Al, Fe, and Mg (refer to DTN: LL000123351021.117 for magnesium data which was not tabulated in Table 3, but follows the same filtration behavior as Al and Fe) and some Si was filterable. The filtration results indicate a colloidal material composed of silica, aluminum, iron and magnesium. These ICP-MS solution results confirm the clay composition of the colloids determined from numerous corrosion tests using TEM (DTN: LL991110251021.099, pp. 156-157) and provide evidence that the TEM results are typical for the bulk solution colloids.

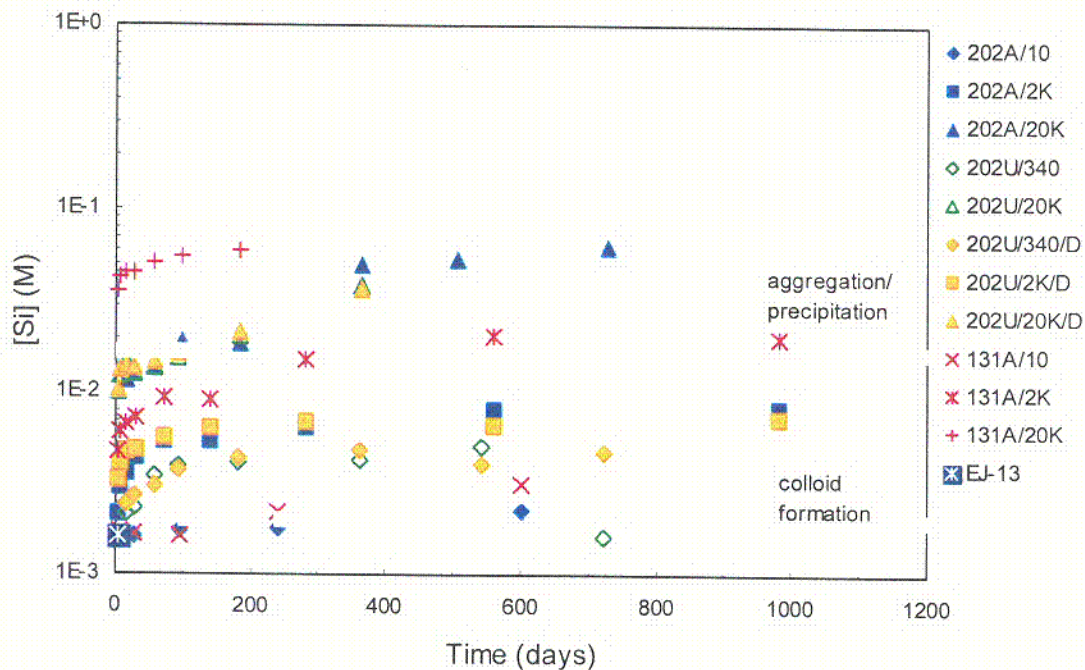
Table 3. Filtrate Concentrations from Filtration through 450 and 6 nm Filters on Leachates from Corrosion Tests with SRL 202U in EJ-13 (20,000/m and 90°C)

Time (days)	pH	Al, ppm < 450nm	Al, ppm < 6 nm	Fe, ppm < 450nm	Fe, ppm < 6 nm	Si, ppm < 450nm	Si, ppm < 6 nm	B, ppm < 450nm	B, ppm < 6 nm
3	11.03	5.34	1.26	26.4	0.38	281	243	76.5	74.3
7	11.02	8.76	1.31	41.2	0.30	344	267	93.3	85.9
14	11.26	11.8	bd	53.4	0.75	414	323	111	107
28	11.38	4.95	1.86	13.4	0.28	356	361	120	127
56	11.39	1.54	na	0.43	na	382	na	148	na
91	11.39	2.33	1.70	0.45	bd	432	443	178	181
182	11.64	1.17	bd	0.17	bd	565	536	245	230
364	11.42	bd	1.20	1.43	2.78	1060	946	3490	3410

NOTE: Average values from duplicate tests are given when available. The bd indicates values below the detection limit, and na indicates the solution was not analyzed (DTN: LL000123351021.117, Table D.3, pp. 254-259).

During the corrosion of high level waste glass under static test conditions, dissolution of the waste form eventually causes the leachate to reach saturated conditions, which promote nucleation of colloids (Geckeis et al. 1998). The silica concentration in the leachates (DTN: LL000123351021.117, pp. 211-259) from several waste glasses (SRL 202A, 202U and 131A) at various surface area of glass to leachate volume ratios was converted to molarity (using the molecular weight of Si). The evolution of the silica concentration as a function of the corrosion of these waste glasses (SRL 202A, 202U, and 131A is shown in Figure 5. Filtration results from the corrosion of the SRL 202A, 202U, and 131A indicate that Pu-bearing colloids are observed at silica concentrations of $\geq 3.5 \times 10^{-3}$ mol/L in low ionic strength solutions (refer to Table 4). This value is above the saturation concentration (1.5×10^{-3} M) determined from leaching experiments on the R7T7 glass at 90°C (Curti et al. 1993). As the dissolution of the glass proceeds and colloids form, eventually the solution composition reaches a critical boundary where the aggregation and precipitation of the colloids occur. Colloids are not observed (or were detected at very low concentrations) in the leachates from the corrosion of the SRL 202A, 131A, and 202U above a silica concentration of $\sim 2 \times 10^{-2}$ M (refer to Table 4) indicating that the colloids aggregated and precipitated out of solution. Colloid formation from homogeneous

nucleation of clay phases during static glass corrosion tests is indicated as the dominant mechanism. Dynamic light scattering results on the colloids from the corrosion of the SRL 131A glass confirm aggregation of the colloids (significant increase in colloid size observed at 280 days and a silica concentration of 1.5×10^{-2} M) (DTN: LL991109751021.094, p. 27). Additional discussion of the dynamic light scattering results is given in Section 6.3.1. While the aggregation and precipitation of Pu-bearing colloids occurs at a critical silica concentration, the colloid destabilization is not merely a function of silica solution concentration; other solution properties (especially ionic strength) influence the colloidal stability. The effect of ionic strength will be discussed later in this section.



NOTE: Total silica in solution (colloidal and dissolved) as a function of test duration for static corrosion tests on SRL 202A, SRL 202U, and SRL 131A glasses at 10, 340, 2,000 (2K), and 20,000 (20K) m^{-1} ($T = 90^\circ C$) (DTN: LL000123351021.117, pp. 211-259). The leachant was EJ-13, except when deionized water (D) was indicated in the legend. The saturation concentration of dissolved silica and the critical aggregation boundary correspond to a value of $\sim 2 \times 10^{-3}$ mol/L and $\sim 2 \times 10^{-2}$ mol/L, respectively. The composition of EJ-13 is represented for comparison.

Figure 5. Total Silica in Solution (colloidal and dissolved) as a Function of Test Duration for Static Corrosion Tests on SRL 202A, SRL 202U, and SRL 131A Glasses

C-1

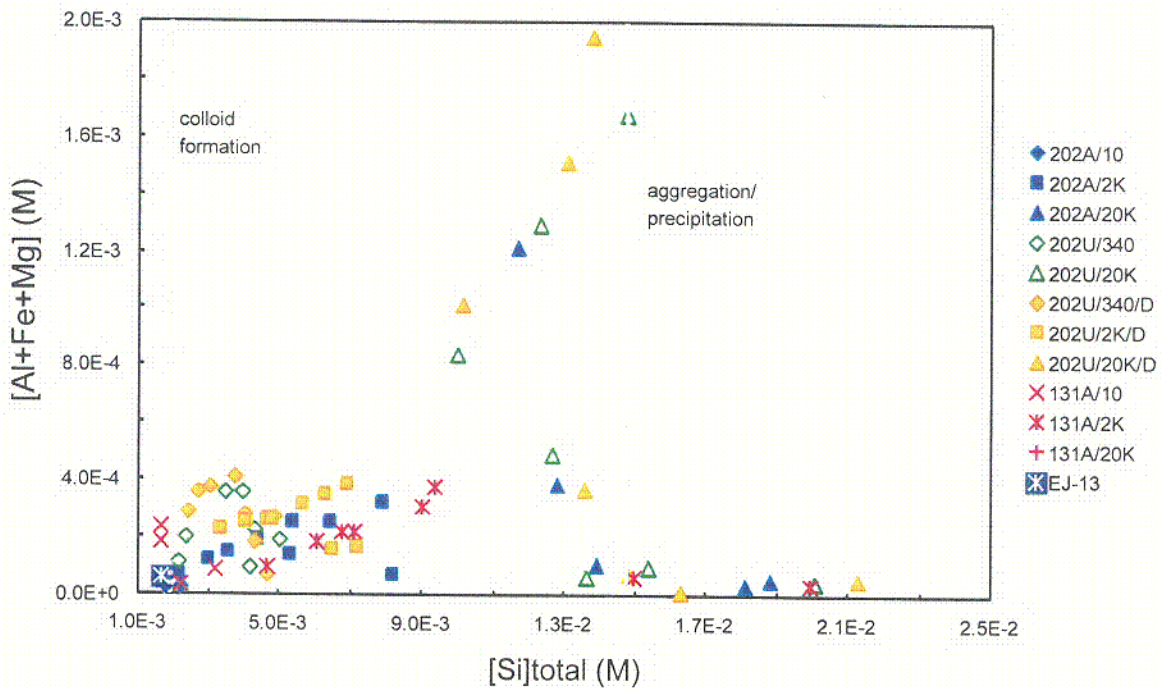
Table 4. Silica Concentration and Mass of Plutonium in Dissolved and Colloidal Fractions of the Leachate from Static Corrosion Tests on the SRL 202A and SRL 131A at Various Surface Area of Glass to Solution Volume Ratios (T = 90°C)

Time (days)	[Si] (M)	Colloidal Pu (ng)	Dissolved Pu (ng)
SRL 202A at 2,000/m			
14	3.51E-03	42	1.8
30	4.38E-03	179	4.1
70	5.27E-03	98	9.9
140	5.36E-03	44	60
280	6.41E-03	109	2.1
560	7.88E-03	80	47
980	8.14E-03	78	18
SRL 202A at 20,000/m			
14	1.17E-02	207	5.0
28	1.28E-02	50	7.8
56	1.39E-02	6.2	1.0
98	1.88E-02	1.2	0.30
182	1.81E-02	1.1	0.15
364	4.90E-02	0.11	0
504	5.30E-02	0	0
728	6.17E-02	0	0.0091
SRL 131A at 2,000/m			
14	6.72E-03	4.3	0.33
30	7.11E-03	5.6	2.0
70	9.36E-03	13.4	7.0
140	9.01E-03	11.6	8.4
280	1.50E-02	1.5	0.32
560	2.06E-02	0.049	0.032
980	2.00E-02	0.007	0.028
SRL 131A at 20,000/m			
14	4.44E-02	0.29	0.0030
28	4.44E-02	0.030	0.0022
56	5.01E-02	0.015	0.0019
98	5.45E-02	0.058	0.0076
182	5.92E-02	0	0.024

NOTE: Pu Data from DTN: LL000122051021.116 and Si data from DTN: LL991109751021.094 (p. 26)

The Al, Fe, and Mg concentrations in solution are found to be predominantly associated with the colloidal phase (refer to Table 2 for Al and Fe data; Mg data not shown; DTN: LL991109751021.094, p. 29). The aluminum concentration in the unfiltered water has previously been used as an indicator of clay colloidal material (Degueldre et al. 1999). A plot of the sum of Al, Fe, and Mg concentrations as a function of total silica in solution (colloidal +

dissolved species) for the three glass compositions and a range of test conditions is shown in Figure 6. Colloids were found in solution between the total silica concentrations of 2×10^{-3} and 2×10^{-2} mol/L (DTN: LL991109751021.094, p. 29). Although the colloid formation and stability correlate with the silica concentration, other parameters such as ionic strength can also describe these transitions (DTN: LL991109751021.094, p. 29). Thus, the silica concentration alone can not describe the colloid behavior. From the data in Figure 6, there appears to be a direct relationship between the sum of the leachate concentrations of Al+Fe+Mg and the Si concentration for the formation of colloids indicating nucleation of smectite clay colloids in solution. As the glass corrodes and the Si concentration increases, eventually the critical aggregation boundary is reached where the colloids are no longer stable in solution most likely due to reduction of the surface charge of the colloids in high ionic strength solutions (van Olphen 1977; McCarthy and Degueldre 1993).



NOTE: Sum of Al, Fe, and Mg concentrations as a function of total silica in solution (colloidal and dissolved) for static corrosion tests on SRL 202A, SRL 202U, and SRL 131A at various S/V ($T = 90^\circ\text{C}$). The S/V (in m^2) used in the tests were: 10, 340, 2,000 (2K), or 20,000 (20K) as noted in legend. The leachant used in the tests was EJ-13 or DIW (EJ-13 was used unless indicated by D in the legend). The saturation concentration of dissolved silica and the critical nucleation boundary correspond to a value of $\sim 2 \times 10^{-3}$ mol/L and $\sim 2 \times 10^{-2}$ mol/L, respectively. The composition of EJ-13 is represented for comparison (DTN: LL991109751021.094, pp. 27-29).

Figure 6. Sum of Al, Fe, and Mg Concentrations as a Function of Total Silica in Solution (Colloidal and Dissolved) for Static Corrosion Tests on SRL 202A, SRL 202U and SRL 131A at Various S/V ($T = 90^\circ$)

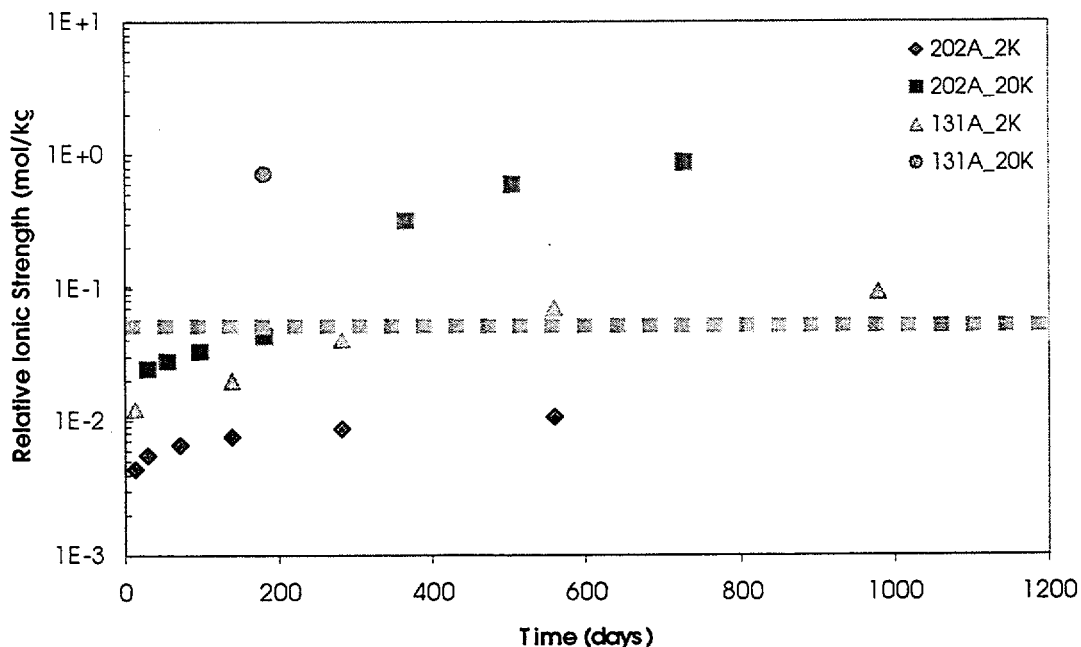
At the pH values of these tests (8 to 12), smectite clays would be highly negatively charged (point of zero charge, pzc of 2.5) and stable in solutions of low ionic strength (Buck and Bates 1999; van Olphen 1977). However, high ionic strength solutions will destabilize and promote

C-2

aggregation and flocculation of the colloids. The ionic strength of the leachate was calculated from the major elements in solution (Li, B, Na, Mg, Al, K, Ca, and Fe) and singly charged hydroxide species were assumed to exist for Al, Fe, B, and Si species at the leachant pH values (as reported previously by Buck and Bates 1999). The elemental concentrations of the major elements (DTN: LL000123351021.117) were converted from ppm to mol/kg, then the ionic strength was calculated using the following formula:

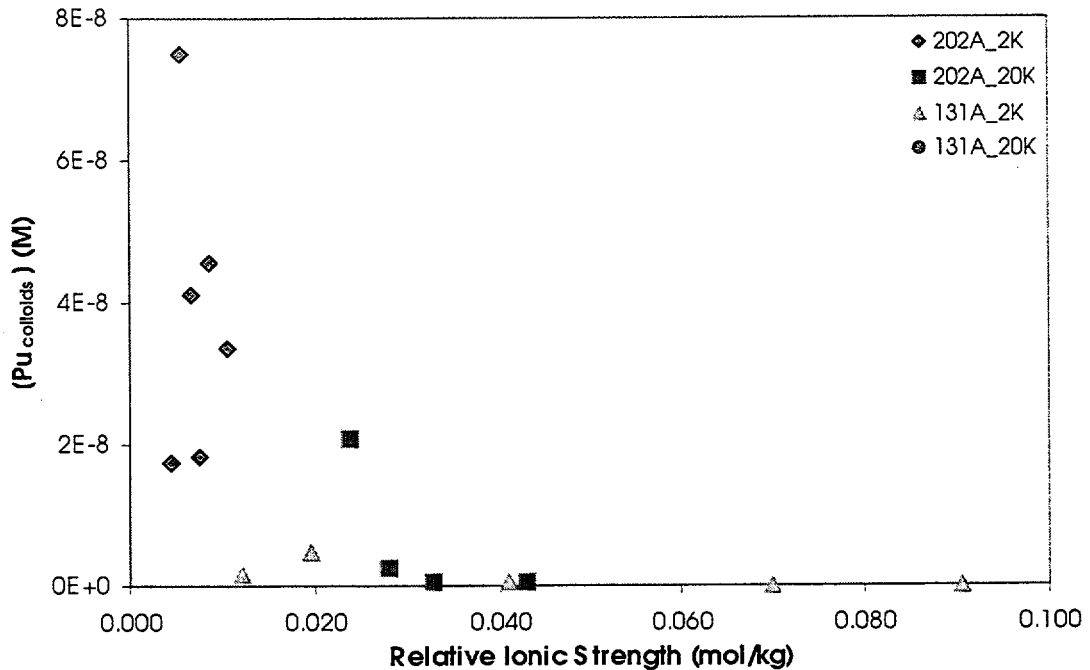
$$\text{Ionic Strength (mol/kg)} = \Sigma[0.5 * \text{concentration of species}_i \text{ (mol/kg)} * (\text{charge of species}_i)^2].$$

The ionic strength increases as the glass corrodes for the SRL 202A and SRL 131A glasses at 2,000 and 20,000/m (shown in Fig. 7). In order to examine the stability of the colloids as a function of ionic strength, a comparison of the ionic strength and the plutonium colloid concentration was performed (DTN: LL000122051021.116; Pu concentration was converted to mol/L using leachate volume and molecular weight of Pu). Figure 8 shows the stability of the plutonium-bearing colloids in low ionic strength solutions. A high fraction of colloids is present in low ionic strength solutions, and the concentration of radionuclide-bearing colloids decreases significantly as the ionic strength is increased (absence of colloids noted for ionic strengths above ~0.05 mol/kg). The observation that low ionic strength favors colloid formation and stability is supported by other studies (Olofsson et al. 1982; Kim 1994; Buck and Bates 1999). While the ionic strength in Figures 7 and 8 was approximated from major components in the leachate (DTN: LL991109751021.094, p. 29), it is used to represent the relative trend as a function of ionic strength, where calculated values based upon solution speciation from a geochemical code would more accurately estimate the ionic strength of these solutions.



NOTE: DTN: LL000123351021.117

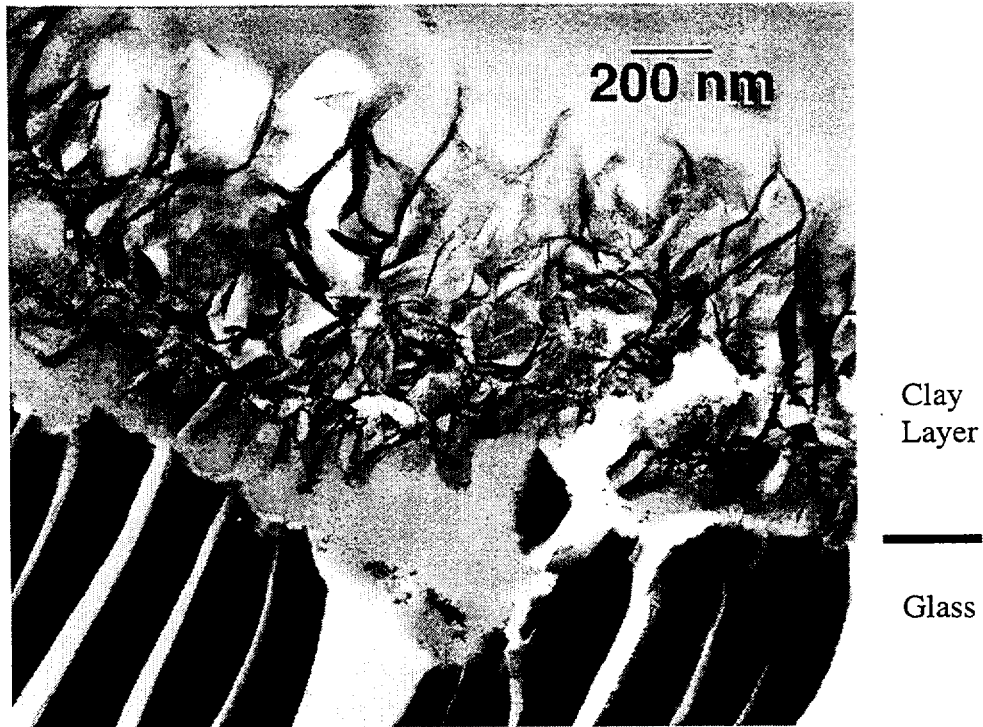
Figure 7. Ionic Strength as a Function of Glass Corrosion for SRL 202A and SRL 131A at 2,000 and 20,000/m (T = 90°C)



NOTE: DTN: LL000122051021.116; LL000123351021.117

Figure 8. Plutonium Concentration from Plutonium-Bearing Colloids as a Function of Ionic Strength for Corrosion Tests on SRL 202A and SRL 131A at 2,000 and 20,000/m (at 90°C)

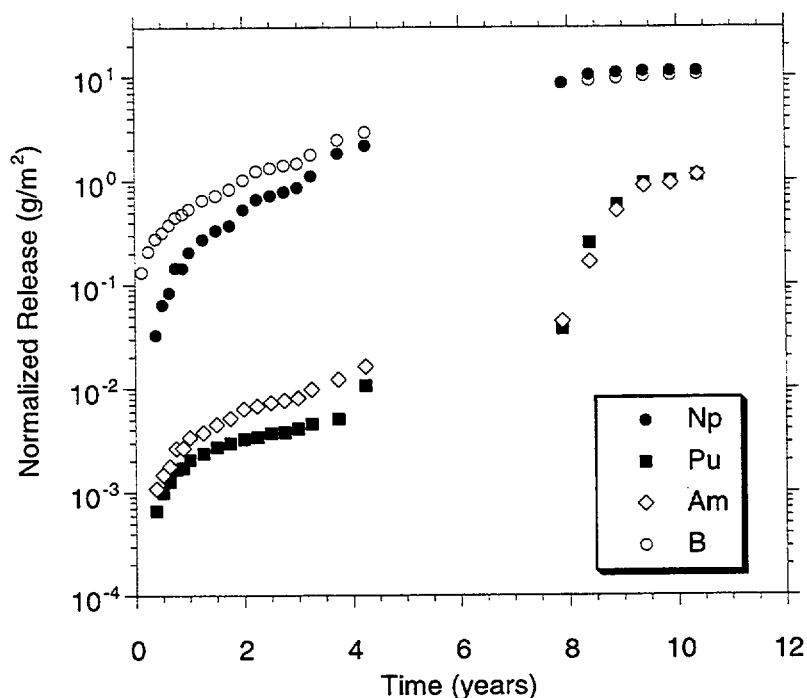
During corrosion of the waste glass, the clay alteration phase nucleates; a layer forms on the surface of the glass, continues to grow and evolves. Growth occurs as the hydrated layer beneath the existing clay dissolves and the elements from solution saturate and reprecipitate onto the surface of the clay. This growth mechanism leads to the observed “backbone” structure of the clays in the N3 test glasses (Fortner et al. 1997a). The very thin clay layers observed early in a test tend to have lattice planes somewhat oriented parallel with the surface, suggesting the original restructuring of the gel at the gel-water interface. At later times (Fig. 9), the majority of the clay lattice is oriented perpendicular to the original glass surface (now the backbone layer), characteristic of growth from solution rather than solid state transformation. Voids are frequently observed between the clay and glass. The etching of the glass beneath the clay continues in an irregular manner, leaving some points of contact between the clay and glass, holding the layer in place. This layer may spall away, however, as stress builds up in the structure and as the glass etches away. This is likely the origin of the clay colloid particles observed in solution from the N3 Drip Tests (Buck and Bates 1999; Fortner et al. 1995, 1997a, 1997b; Fortner and Bates 1996).



Note: DTN: LL991110651021.103 (pp. 46-47)

Figure 9. The Clay Layer on Glass after 38 Weeks of Testing in the N3 Series

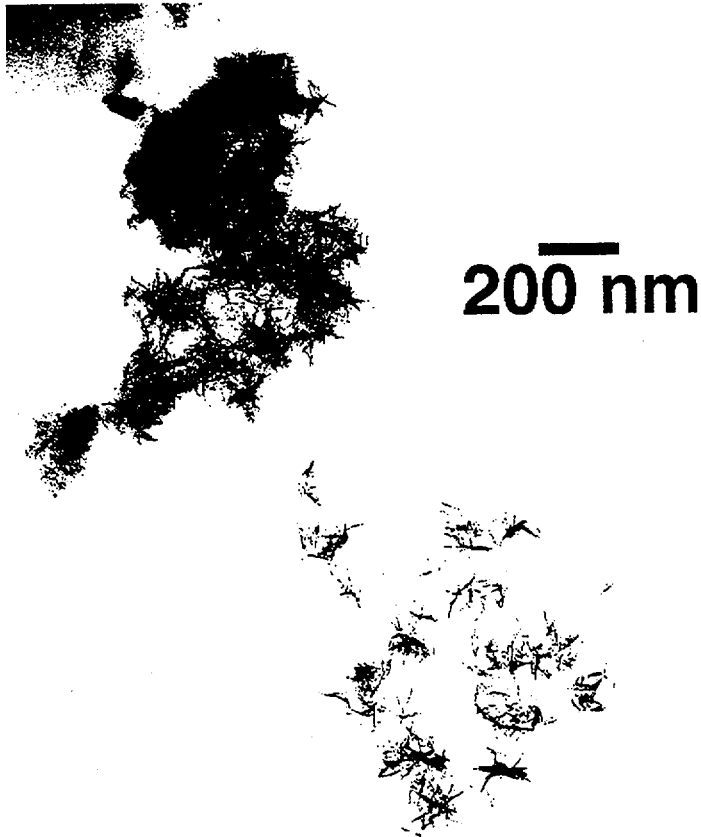
The apparent role of colloids in actinide release in the drip tests is illustrated in Figure 10. Here, the cumulative normalized release (from unfiltered test solution) of the elements B, Np, Pu, and Am from one of the three ongoing tests in the N2 Series displays a behavior that is best explained by a release of particulate material to solution. The soluble elements B and Np were initially released at a substantially greater rate than the relatively insoluble elements Pu and Am. The sudden increase in the release of the insoluble elements Pu and Am shortly after 400 weeks is strong evidence that alteration phases can spall from the corroded glass surface generating a broad range of particulate material believed to range from large flakes (suspended material larger than colloids) to colloids. The fraction of suspended material that was greater in size range than colloids was not determined. Almost no Am or Pu appears in the filtered solution, while the Np in the filtered solution is essentially the same as that in the unfiltered. The spallation of alteration phases, some of which have incorporated Pu and Am, most likely led to total cumulative release of these elements. Some potential actinide-bearing alteration phases have been observed using analytical electron microscopy (AEM). Many of these particles have small ($< 1 \mu\text{m}$) linear dimensions and high surface areas characteristic of colloids. The following examples of these particles, plus others from the N3 and N4 series, are described in detail.



NOTE: DTN: LL000205551021.118

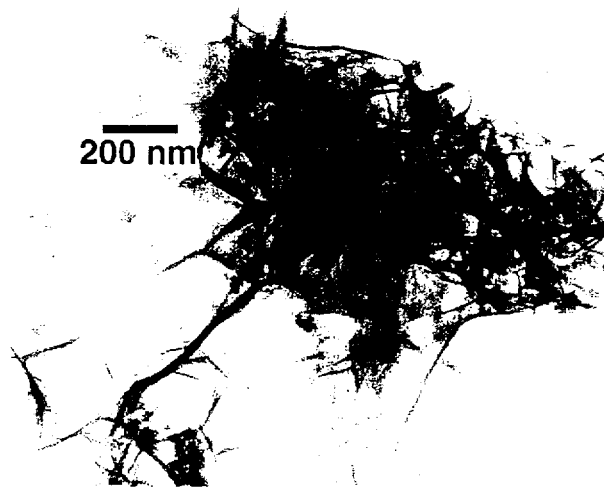
Figure 10. The Cumulative Normalized Release of the Elements B, Np, Pu, and Am from One of the Tests in the N2 Series

In both the N2 and N3 tests, the majority of colloidal particles observed by AEM have been either smectite-type clay or a variety of iron-silicates (Fig. 11). Both clays and iron silicates can sorb actinides, and, thus, these colloids represent potential transport mechanisms for insoluble elements. In the N2 tests, both the clay and iron-silicate colloids are sometimes observed to contain small amounts of uranium. Uranium is also observed on occasion in the clays and iron-silicates from the N3 tests; thorium is generally detected only in an entrained alteration phase such as the thorium calcium orthophosphate mineral, brockite, and not in the clay itself. Examples of brockite-containing colloids, including evidence for their high transuranic content, appear in Figure 12. The 200R glass in the N4 drip test also produced a brockite-like alteration phase rich in REE (Fig. 13). None of the above colloid particles were observed in a wicked solution from the blank tests.



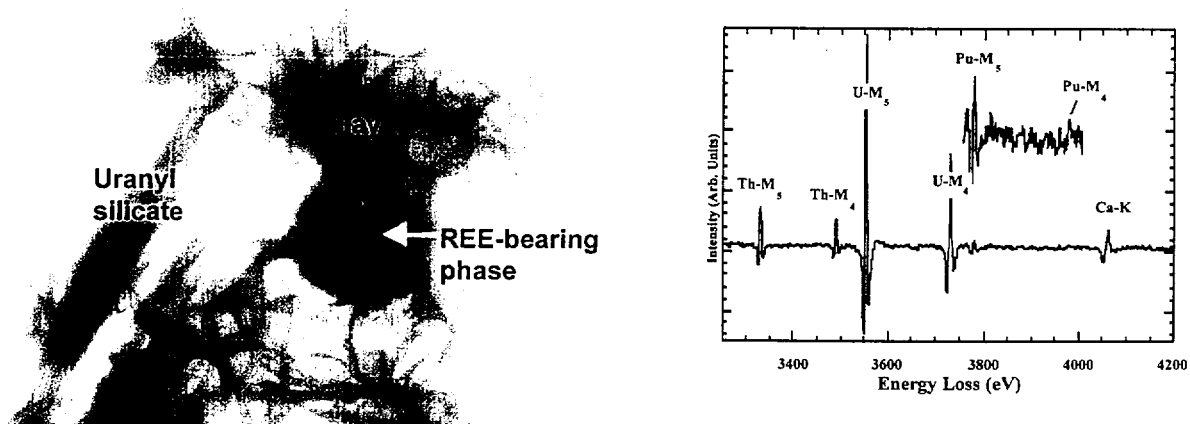
NOTE: DTN: LL991110451021.101 (p. 147, sample: N2-12, test sampled: 12-8-95)

Figure 11. Transmission Electron Microscopy Micrograph of Clay Colloid Particles Extracted from the Glass Drip Tests



NOTE: DTN: LL991109951021.096 (pp. 126-127)

Figure 12. Smectite Clay Colloids from the N3 Glass Drip Tests with Entrained Particles of Brockite (dark regions within clay matrix)



NOTE: At left is a TEM image of a REE-bearing phase from a 200R glass drip test (DP98, DTN: LL991109951021.096, p. 104). The EELS analysis of the particle (right) demonstrates that it contains actinide elements (DTN: LL991109951021.096, p. 161; DTN: LL991110451021.101, pp. 106-107).

Figure 13. TEM Image and EELS Analysis of a REE-Bearing Phase from a 200R Glass Drip Test (N4)

The mechanism for the spalling of clay particulates and colloids from the glass surface is not clear. The microscopic examination of the corroded glass surfaces from the N3 drip tests may provide important clues (see, for instance, Fig. 9). Voids are frequently observed between the clay and glass, a result of either disproportionate growth/dissolution rates or accumulating strain due to different materials properties between the glass and the clay layer. The etching of the glass beneath the clay continues in an irregular manner, leaving some points of contact between the clay and glass, holding the layer in place. This clay layer may spall away, however, as stress builds up in the structure and as the glass etches away beneath. This is likely the origin of the

clay colloid particles observed in solution from the drip tests. Therefore, as the clay becomes detached from the glass, actinide-bearing alteration phases may be released. This results in the delayed release of Pu and Am as suspended particles (DTN: LL000205551021.118). However, owing to the low concentrations, the transuranic content of the specific phases cannot be determined with TEM.

The source of primary colloids in the unsaturated tests is the altered surface of the glass. In order to characterize the source of these colloids, sections of the reacted surface plus alteration phases were removed from the N3-9 and N3-10 glass monolith surfaces during the July 1995 sampling of the N3 tests. The appearance of the N3-10 glass monolith at this time appears in Figure 14, where the surface alteration layer has spalled a fragment of clay, revealing underlying glass.

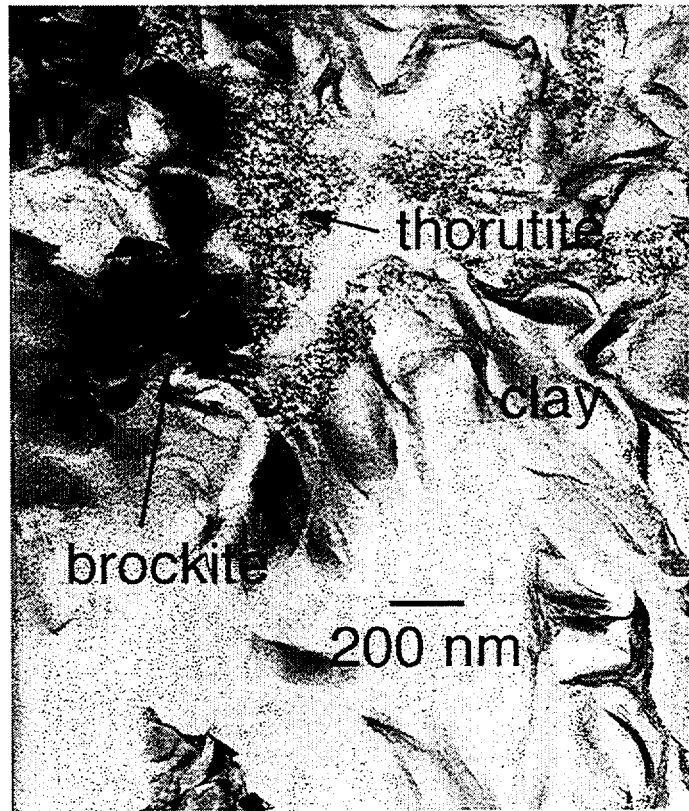


NOTE: Fragments of clay alteration layer have broken off, revealing underlying glass. Note the nascent growth of new clay in the spalled regions (DTN: LL991110751021.104, pp. 84-85).

Figure 14. The N3-10 Glass Monolith after about 8 Years of Testing

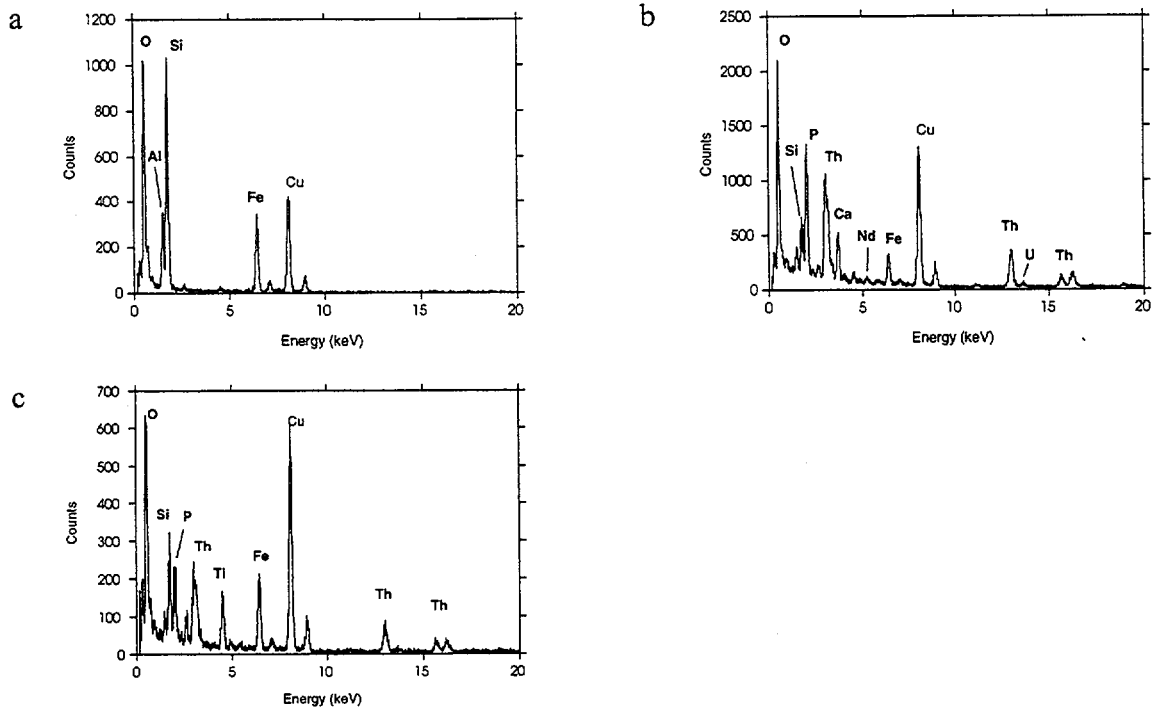
The particles removed from the N3 surfaces included mostly clays with discrete alteration phases within the clay layer. Among the discrete phases were many brockite particles and an amorphous thorium-titanium-iron silicate, similar to the mineral thorutite (nominally, [Th, U, Ca] Ti_2O_6). REE and actinides are found within these discrete phases and, if spalling of the clay layer occurred, would allow the transport of these phases with the clay. While TEM was limited in detection of Pu by its low concentrations in the glass, the behavior of plutonium and americium is expected to follow that of the rare earths and the actinides. A transmission electron micrograph of a portion of this N3 clay matrix material appears in Figure 15. The chemical compositions of the individual phases are characterized by the EDS spectra of Figure 16, while EELS analysis of REE and actinides in the brockite appears in Figure 17. The distribution of rare earths and actinides at 8 years is virtually identical to that observed in tests terminated after

1 year (Fortner et al. 1995, 1997a). At one year, very little spallation was observed in terminated test glass surfaces (Fortner et al. 1995, 1997a).



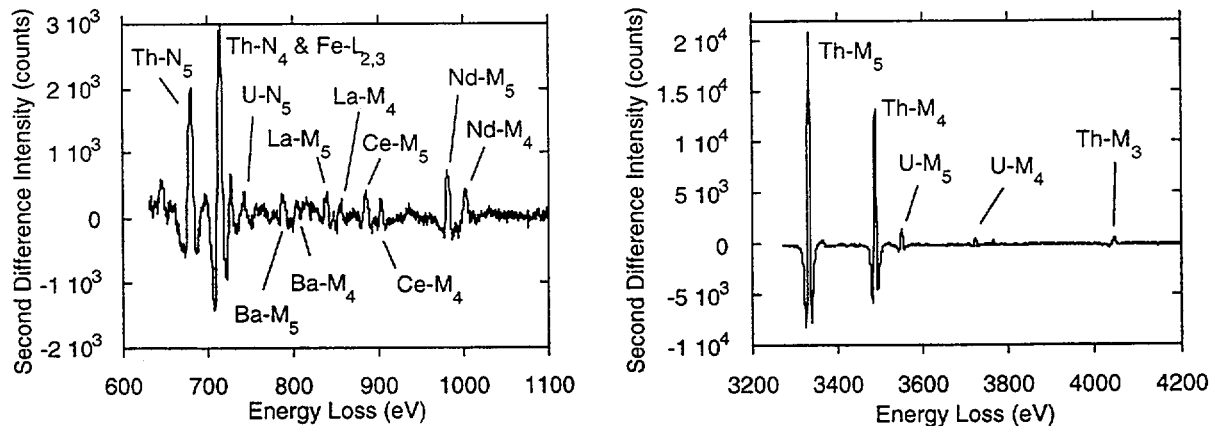
NOTE: The clay alteration layer on the N3-10 glass, sampled July 1995 after approximately 8 years of testing, was found to consist of a composite of smectite clay, brockite crystallites, and thorutite as seen in this transmission electron micrograph. The thorutite is a titanium-iron-thorium precipitate that forms in the solution between the layer and the dissolving glass and is trapped by the clay layer (DTN: LL991110451021.101, pp. 3-5).

Figure 15. The Clay Alteration Layer on the N3-10 Glass after approximately 8 Years of Testing



Note: The three components comprising the N3-10 clay composite were examined using EDS in the AEM, providing the above spectra of (a) smectite clay, (b) brockite, and (c) an amorphous Th-Fe-Si-Ti phase (similar to thorutite). The copper lines are an artifact of the sample mount. The EDS spectra of these phases accompany the labels in Figure 15 (DTN: LL991110451021.101, pp. 3-5).

Figure 16. EDS Spectra of the Three Components Comprising the N3-10 Clay Composite



NOTE: EELS spectra of the brockite phase from the N3 sample shown in Figure 15 showing REE and actinides as in brockite particles from tests terminated at times of one year or less (DTN: LL991110451021.101, pp. 3-5).

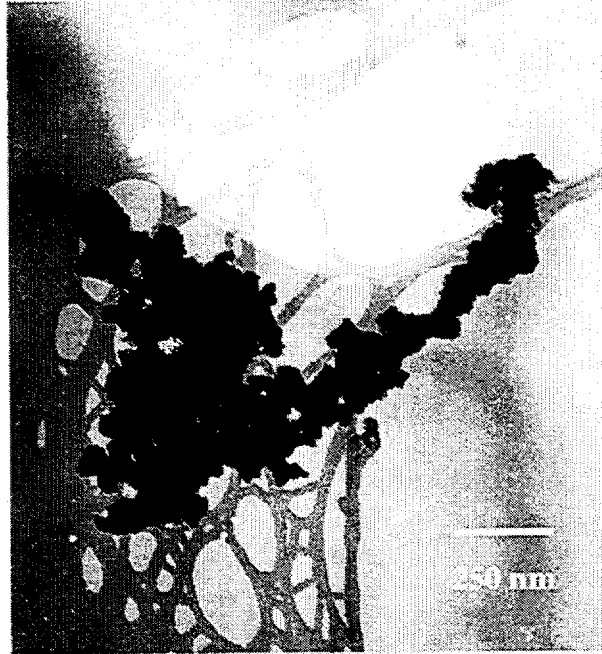
Figure 17. The EELS Spectra from the Brockite Particles

6.2.2 Colloids Generated from Spent Fuel Corrosion

This section will focus on the detection and identification of colloidal species generated during long-term intermittent drip tests on the spent fuels (ATM-103 and ATM-106) and UO_2 . During oxidative dissolution of spent fuel, U^{6+} secondary phases (uranyl oxide hydrates, uranyl silicates, phosphates, or carbonates) are known to form, which are dependent on the composition of the contacting fluid. Spent fuel with its complement of fission and neutron capture products may also allow the precipitation of alteration phases of insoluble elements depending on their availability in the fuel matrix. For example, plutonium, owing to its low solubility in groundwaters, can form discrete plutonium phases that can contribute to the colloid inventory.

Corrosion tests with two types of well-characterized spent fuel from pressurized water reactors have been conducted: ATM-103 with a burnup of ~ 30 MWd/kgU and ATM-106 with a burnup of ~ 45 MWd/kgU. The experiments were conducted in stainless steel (type 304L) vessels. A small amount of EJ-13 water (5 ml) was deposited in the base of the vessel at the start of the tests and after each sampling to ensure 100% relative humidity at all times. The spent fuel was placed inside a Zircaloy-4 sample holder. The holder consisted of a 1.33 cm diameter tube, which contained a 20 μm thick filter with 10 μm diameter holes. A small quantity of EJ-13 water (0.75 ml) was injected every 3.5 days from a reservoir onto the top of the spent fuel in the holder. Air was flushed through the lines to force water left in the lines onto the fuel. Further details on the tests can be found elsewhere (Finn et al. 1994a).

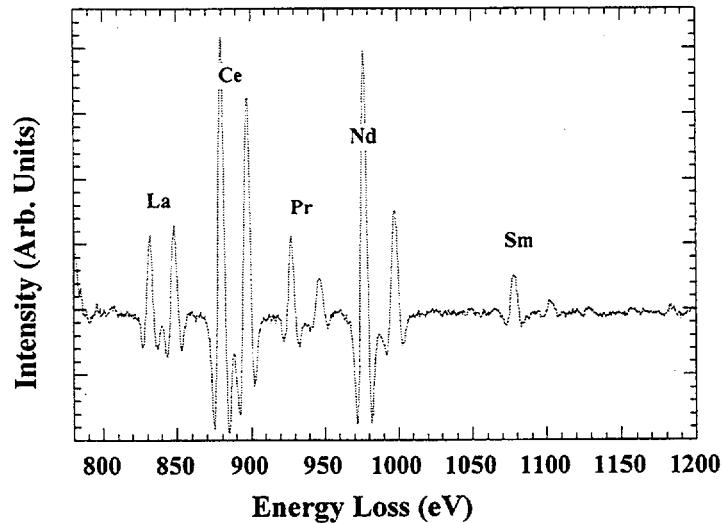
Compared to glass tests, very little radionuclide-bearing colloidal and suspended particle material was found from TEM examinations of the spent fuel test samplings. Data from other waste form corrosion drip tests, including those conducted with UO_2 (Wronkiewicz et al. 1996; Buck and Bates 1999), suggest that colloids may be produced from spallation of the reacted waste form. Two radionuclide-bearing phases were found in the spent fuel colloids detected during the ATM-103 high drip rate sampling at 57 days (DTN: LL991110251021.099, pp. 67-69, sample: S32J1-57NF). The uranium to silicon ratio in these two phases appeared to vary (very little Si in one and 1:1 ratio in the other). Partially crystalline uranium silicate colloids (Figure 18) were identified in the sample. Selected area electron diffraction (SAED) analysis and x-ray EDS compositional data identified the colloid as soddyite, a uranyl silicate with a U/Si ratio of 1:1 (Finn et al. 1994a).



NOTE: The particles were polycrystalline uranium-bearing phases with a high concentration of silicon (Finn et al. 1994a; DTN: LL991110251021.099, pp. 67-69).

Figure 18. Bright-Field TEM Image of Particles from 57 Day Sampling from an ATM-103 Test

Figure 19 shows an EELS spectrum for the second uranium-bearing colloid phase, which contained very little silicon. The EELS determined that the colloids contained the REEs: La, Ce, Pr, Nd, and Sm (Fig. 19). Compositionally, similar particles were also found in the ATM-106 low drip rate tests (DTN: LL991110851021.105, pp. 42-44, sample: S61J1-127). The REE were not uniformly distributed in the uranium colloids but were concentrated in the uranium phases. While no detectable plutonium was observed in these colloidal particles, rare earth-bearing particles were observed on the surface of the corroded spent fuel which contained significant amounts of plutonium. The uranium-bearing phase at the surface of the corroding fuel containing the REEs was crypto-crystalline, and the morphology consisted of 20-50 nm particle agglomerates (DTN: LL991110251021.099, p. 80, sample: S32J1-57).

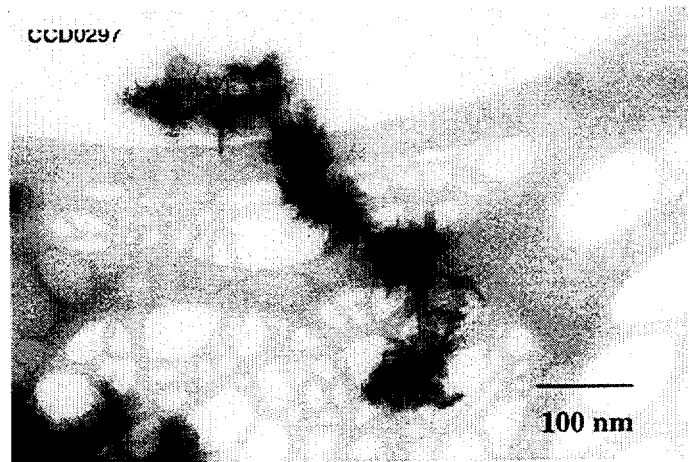


NOTE: Electron energy-loss spectroscopy of colloid from the high-drip-rate test on the ATM-103 was sampled at 57 days. The colloid was rich in REE but did not contain Pu (DTN: LL991110251021.099, p. 80, sample: S32J1-57).

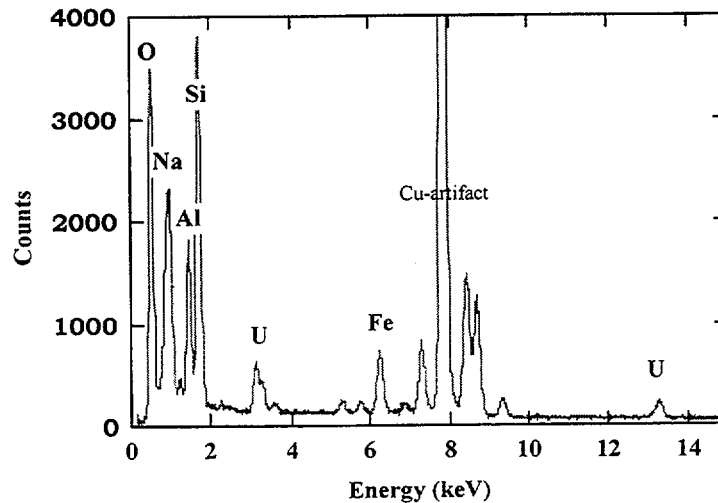
Figure 19. Electron Energy-Loss Spectroscopy of Colloid from S32J-57

In Figure 20, a micrograph shows the most common phase observed in the ATM-106 high-drip-rate sampling at 747 days (DTN: LL991110051021.097, p. 182, sample: S62J1-747). This phase was identified by electron diffraction as smectite clay. The EDS analysis of the smectite type clays for the spent fuel tests indicated that they contained significant quantities of manganese, as well as nickel with smaller amounts of iron and trace chromium (Fig. 20b). The transition metals may have come from various test components or the groundwater drip solution (EJ-13). The diffraction patterns also reveal a possible double ring structure in the $hk0$ reflections—perhaps only a slight broadening of the peaks. This has been found to be typical of the layer Mn oxide and Ni oxide minerals (such as birnessite). (Birnessite has been observed in other samples, particularly associated with the clay minerals observed in the N4 glass tests [Buck and Bates 1999].) The clays found in the spent fuel tests do appear to be similar both in composition and structure to the clays found in the glass tests. This is supporting evidence that clays are a major colloidal particle in all corrosion tests.

20(a)



20(b)

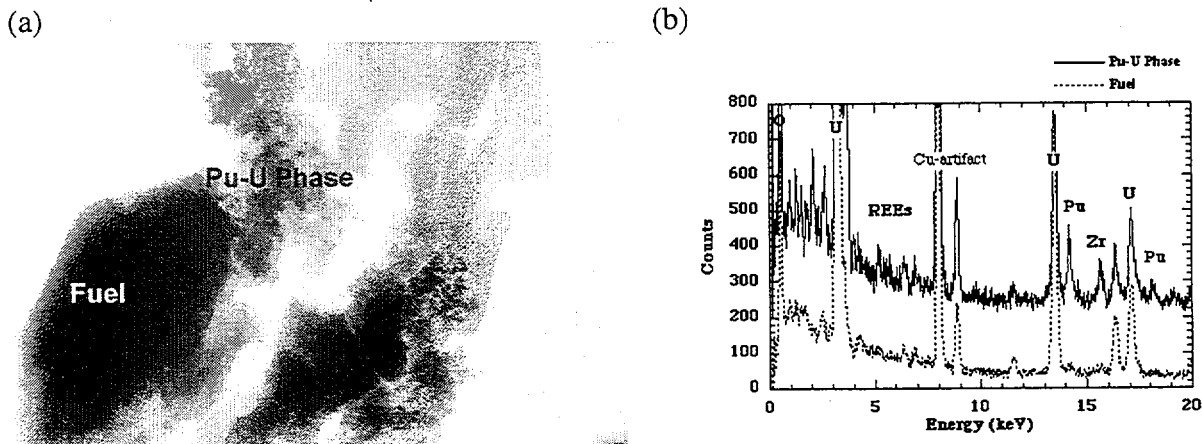


NOTE: Sample: S62J1-747 (DTN: LL991110051021.097, p. 182) and sample: S32J1-748 (DTN: LL991110051021.097, p. 182)

Figure 20. (a) Example of Smectite Clay Colloids from Corrosion Test with ATM-106 and (b) X-ray Energy Dispersive Analysis of Clay Colloid from an ATM-103 Test

During the TEM examination of corroded ATM-103 fuel from both the vapor and high-drip tests, regions were found which possessed anomalously high concentrations of plutonium (see Fig. 21). The Pu-rich regions were small (100 nm thick) and may even be considered colloidal aggregates within the alteration layer. The material did not possess the microstructure typical of a uranyl alteration phase but was cryptocrystalline. X-ray energy dispersive analysis indicated that the concentration of plutonium in the phase was relatively high. The phase also contained Zr and Ru, as well as a series of REE. Analysis of the phase with EELS revealed a distribution of REE, which matched the distribution of these elements in the unreacted fuel within the precision of the EELS measurement. Two explanations for the occurrence of the Pu-rich residues in the corroded SNF are plausible. These phases could have been in the fuels before

testing commenced (i.e., they formed in the reactor), or they may result from the accumulation of insoluble material on the surface of the corroding fuel.



NOTE: Transmission electron microscopy image (Figure 21a) of Pu-rich regions within the corroded ATM-106 fuel reacted under high-drip-rate conditions for 5 years (DTN: LL991110351021.100, p. 36, sample: S61J1-49m). Compositional analysis of the fuel and altered regions is shown in Figure 21b (DTN: LL991110351021.100, p. 36, EDS13314, EDS13317). The alteration phases were identified as a calcium uranyl oxide hydrate and a Cs-Mo uranyl oxide hydrate. Compositional EDS analysis of the corroded sample and the fuel showing enriched levels of Pu, Ru, and Zr relative to the uncorroded fuel.

Figure 21. (a) Transmission Electron Microscopy Image of Pu-Rich Regions within the Corroded ATM-106 Fuel Reacted under High-Drip-Rate Conditions for 5 Years and (b) Compositional Analysis of the Fuel and Altered Regions

The plutonium enrichment levels in these residues far exceeded those reported in the uncorroded ATM-103 and ATM-106 fuels. In high burnup fuels, so-called “grey phases” consisting of Ba, U, Pu, Zr, and Mo have been found. These are perovskites with the general formula $[(Ba_{1-x-y}Sr_xCs_y)(U,Pu,RE,Zr,Mo)O_3]$, which are formed in the reactor during operation. However, the Pu-rich residues are thought to be formed during dissolution of the fuel, based on the location of these phases in the corroded fuels, and the fact that such phases were not observed during the initial fuel characterization by Thomas et al. (1992). The TEM analysis of the Pu-residues indicated significant levels of Zr, Ru, and lesser amounts of REE. The U:Pu ratio was approximately 1:0.3.

Because these phases have been observed in several different tests under different conditions with both ATM-103 and 106 fuels, they are thought to be formed during dissolution. In Figure 21, the location of the Pu-layer is the strongest evidence supporting the idea that this material has formed during the oxidative dissolution of the fuel. The Pu layer is sandwiched between uranyl alteration phases and the fuel. This layer is only 100 nm thick, which explains why it has not been observed in the SEM.

The presence of enriched regions of Pu suggests that if these regions become friable, Pu-bearing colloids could be released; however, through 6 years of testing there is no evidence that these types of particles are released into solution.

Particles of both alteration phases and UO_2 were observed in the leachate from the UO_2 drip tests started several years before the spent fuel drip tests (Wronkiewicz et al. 1996). The open form of the sample holder may have permitted particles to more easily enter the collection vessel than the spent fuel tests. Uranium silicate particles were found in the leachates of seven-year UO_2 tests (Wronkiewicz et al. 1996). The particles were elongated, displaying a morphology typical of a uranium silicate. The phase was identified as uranophane, a uranyl silicate, ideally $[\text{Ca}(\text{H}_3\text{O})_2(\text{UO}_2)_2(\text{SiO}_4)_2 \cdot 3\text{H}_2\text{O}]$ which has a Si:U ratio of 2:1.

6.3 SIZE DISTRIBUTION OF WASTE FORM COLLOIDS

This section provides analyses that summarize the size distribution of radionuclide-bearing colloids generated from the corrosion of high level waste glass and commercial spent nuclear fuel. The methods employed for colloid characterization in this section are DLS and filtration (analysis of filtrates with ICP-MS or alpha spectroscopy). Data used in these analyses include filtration data from several years of static glass tests (DTN: LL000122051021.116; LL000123351021.117) and filtration data from 1.6 to 4.8 years of spent fuel tests (LL991001251021.090). Limited dynamic light scattering data on waste form colloids are available from glass (DTN: LL991109751021.094, p. 32) and spent fuel tests (DTN: LL991109751021.094, p. 34). The DLS technique was not available for many of the early testing analyses and has not been used extensively to study the glass corrosion colloids. The bulk solution clay colloids formed during glass corrosion have been correlated with the Pu in the colloid phase using filtration and DLS data presented in this section. While the filtration and DLS measurements cannot distinguish between the type of colloids formed, TEM has identified discrete radionuclide-bearing phases incorporated in the clay colloid matrix. In low ionic strength solutions, the colloids formed during the corrosion of waste glass have a wide distribution with a mean diameter of 120 to 160 nm (DTN: LL991109751021.094, pp. 30, 32). The glass waste form colloids are destabilized in high ionic strength solutions and colloid concentrations are negligible (DTN: LL991109751021.094, pp. 30, 32).

Dynamic light scattering is a non-destructive technique for determining the particle size of colloids in solution. Data analysis was performed with well accepted methods, cumulants and Contin (Johnsen and Brown 1992). The cumulants method is limited to narrow size distributions and assumes a spherical particle. For wide particle distributions, Contin has been employed to avoid the bias of fixed-form models and provide reliable information on the particle size distribution. Measurement durations are several minutes for strongly scattering samples and are strongly influenced by dust or other contaminants when low colloid concentrations are present. Generally, the minimum concentration limit for DLS analyses is 10^7 particles/mL for 100 nm colloids (McCarthy and Degueldre 1993). The detection limit depends on the particle size, scattering efficiency, measurement duration, laser power, and other parameters. Particle sizes can easily be determined at concentrations as low as 0.2 ppm. Concentrations lower than 0.2 ppm can be determined with optimization of the signal-to-noise ratio. The particle concentrations were obtained by comparing the scattering intensity of the samples to those of known concentrations of 70 and 300 nm polystyrene nanosphere standards (which assumes that

the sample scatters light as efficiently as the polystyrene). This assumption is good for the clay colloids from glass corrosion tests where the index of refraction of the polystyrene standards is 1.6 which corresponds well with that of clays ($n = 1.53$ to 1.64) (Schurtenberger and Newman 1993).

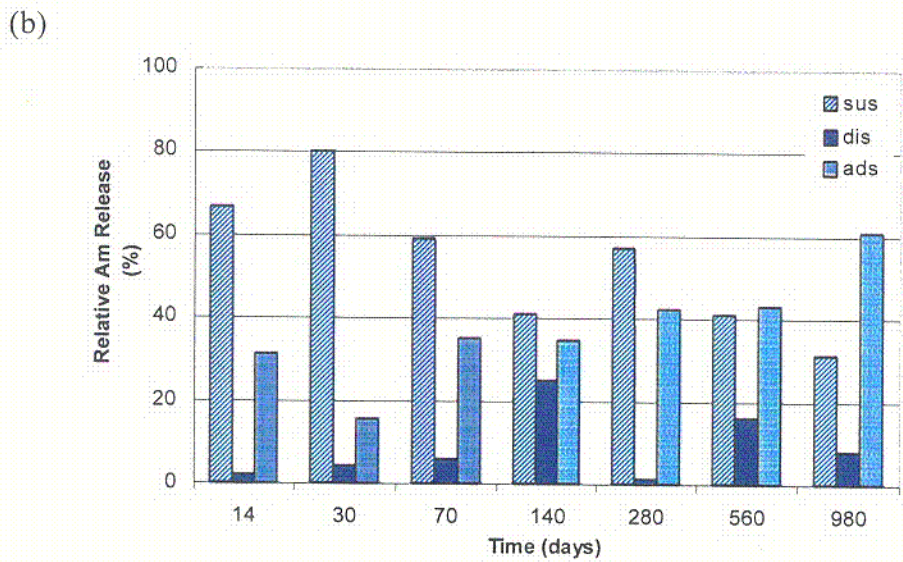
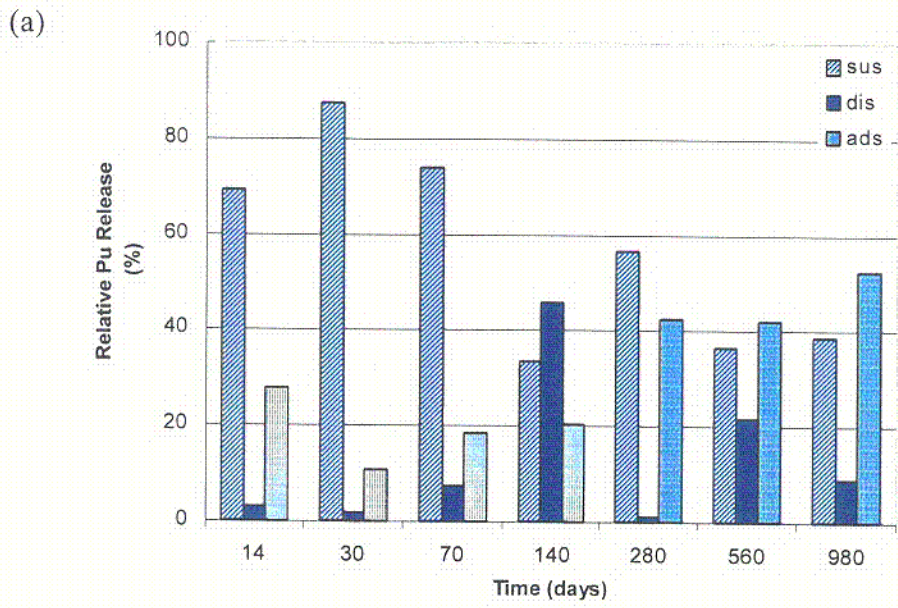
6.3.1 Size Distribution of Colloids Generated from Glass Corrosion

Filtration was performed on the leachates from static corrosion tests on the SRL 202A, 202U, and 131A glasses. Colloidal (450 nm filtrate minus the 6 nm filtrate), dissolved (6 nm filtrate), and adsorbed (acid strip solution) species of plutonium and americium are shown in Table 5 (DTN: LL000122051021.116). The percent of radionuclides associated with various size fractions was obtained from the filtration results (DTN: LL000122051021.116) by dividing the mass fraction of the radionuclide in each size fraction by the total radionuclide mass fraction released. A representative plot of the filtration data is shown in Figure 22. The filtration results of leachates from the static tests indicate that a large fraction of plutonium (up to 90% of the released Pu) was released initially as colloids from the corrosion of the SRL 202A glass at 2,000/m and 20,000/m. As the corrosion of the glass proceeds, the released plutonium is predominately present as adsorbed material on the test vessel. The americium released during the corrosion of the glass, although at a much lower concentration than the Pu, exhibits the same behavior as the plutonium. A large fraction of colloidal Pu and Am was also released during the corrosion of the SRL 131A glass at 2,000/m; however, the maximum amount of radionuclide-bearing colloids (22%) was lower than for the 202A glass. The adsorbed fraction of released Pu and Am dominated the longer duration and higher S/V tests (20,000/m) with 90-100% of the material being adsorbed. Based on filtration results of the leachate from the corrosion tests on SRL 202U at 20,000/m (Table 3), the colloidal fraction is predominately composed of an aluminum, iron, silica-rich material. This has been observed for the other waste glasses as confirmed by TEM analysis.

Table 5. Percentage of Plutonium and Americium Released as Colloidal (c), Dissolved (d), and Adsorbed (a) Forms in Leachates of Corrosion Tests with SRL 202A and SRL 131A at 2,000 and 20,000/m

Time (days)	Pu_c (%)	Pu_d (%)	Pu_a (%)	Am_c (%)	Am_d (%)	Am_a (%)
SRL 202A @ 2,000/m						
14	69.1	3.0	28.0	66.5	2.2	31.3
30	87.3	2.0	10.7	80.4	4.2	15.5
70	74.0	7.5	18.5	59.2	5.9	34.8
140	33.6	45.8	20.6	40.8	24.8	34.5
280	56.4	1.1	42.5	56.8	1.2	42.0
560	36.5	21.5	42.0	40.9	16.2	42.9
980	38.6	8.9	52.5	31.3	8.0	60.7
SRL 202A @ 20,000/m						
14	90.0	2.2	7.8	86.8	2.1	11.1
28	37.2	5.8	57.0	18.9	5.4	75.7
56	14.7	2.4	82.9	11.3	1.1	87.6
98	1.7	0.4	97.9	1.7	0.1	98.2
182	2.2	0.3	97.5	1.5	0.2	98.3
364	0.1	0.0	99.9	0.1	0.0	99.9
504	0.0	0.0	100.0	0.0	0.0	100.0
728	0.0	0.0	100.0	0.0	0.0	100.0
131A @ 2,000/m						
14	22.4	1.7	75.9	10.8	0.5	88.7
30	11.3	4.0	84.7	11.9	1.6	86.4
70	17.3	9.0	73.6	12.8	6.0	81.1
140	15.7	11.4	73.0	8.6	5.8	85.6
280	1.4	0.3	98.3	1.3	0.5	98.2
560	0.0	0.0	99.9	0.0	0.0	100.0
980	0.0	0.0	100.0	0.0	0.0	100.0
SRL 131A @ 20,000/m						
14	1.7	0.0	98.3	0.6	0.0	99.4
28	0.1	0.0	99.9	0.4	0.0	99.6
56	0.0	0.0	100.0	0.0	0.0	100.0
98	0.0	0.0	99.9	0.0	0.0	100.0
182	0.0	0.1	99.9	0.0	0.0	100.0
364	0.0	0.0	99.9	0.0	0.0	100.0
552	0.0	0.0	100.0	0.0	0.0	100.0
728	0.0	0.0	100.0	0.0	0.0	100.0

NOTE: DTN: LL000122051021.116



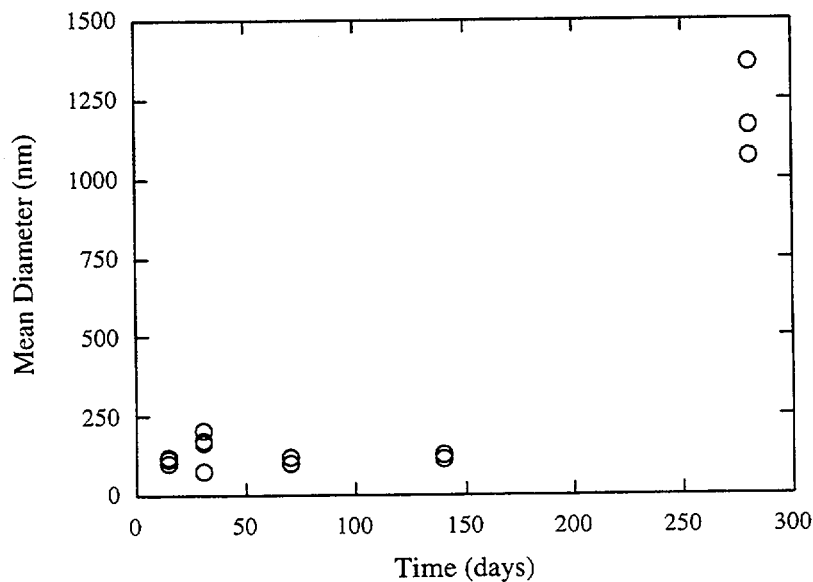
NOTE: The radionuclide was distributed between the various species: 450 to 6 nm as suspended (sus = hatched area), < 6 nm as dissolved (dis = solid area), or adsorbed to test vessel (ads = dotted area) (DTN: LL000122051021.116).

Figure 22. Amount of Plutonium and Americium Released from SRL 202A Static Corrosion Tests at 2,000/m (T = 90°C)

DLS results have been instrumental in correlating the bulk solution colloidal properties with the compositional results from TEM and the radionuclide distribution from filtration. Cumulants analysis of the DLS measurements on the leachates from 14 to 280 days corrosion tests on SRL 131A in EJ-13 at 2,000/m indicated a broad distribution (DTN: LL991109751021.094, p. 32). Due to the large variance of samples, Contin analysis was performed to obtain the mean colloid diameter (Fig. 23). Results from Contin on the leachate solutions for up to 140 days of reaction indicate a wide, monomodal distribution. The mean diameter was 120 nm (with standard

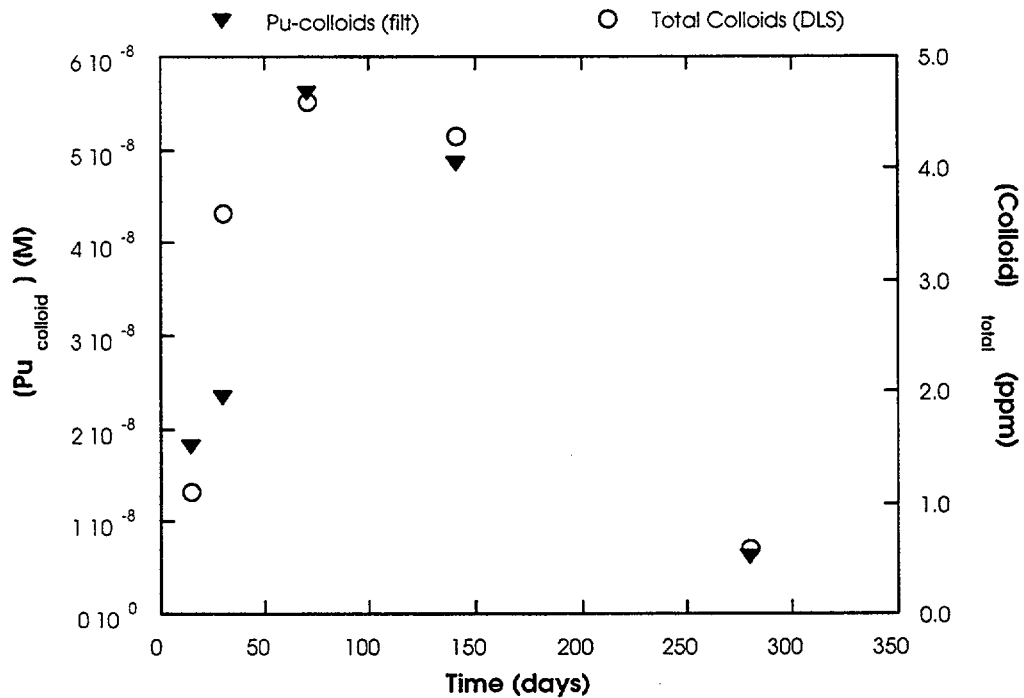
C-3

deviations of 65-90 nm) for the 14, 70, and 140 samples and the 30 day sample was slightly larger with a mean diameter of 160 nm diameter (standard deviation of 100 nm) (DTN: LL991109751021.094, p. 32). Analysis on the 280-day leachate showed a dramatic increase in the particle size to ~1.2 micron (at the upper limit of DLS measurements). The colloid concentration as a function of time is shown in Figure 24 (DTN: LL991109751021.094, p. 33 for DLS measurements and DTN: LL000122051021.116 for the Pu filtration concentrations). The colloid concentration increased to a maximum at ~70 days for both the filtration and DLS results. This correlation between Pu distribution in the leachate (from the filtration and alpha spectroscopy results) and the bulk colloid concentration in the leachate (as determined by DLS) indicates that the colloidal Pu species is associated with the bulk clay colloids.



NOTE: Data analysis was performed with Contin (monomodal distributions) (DTN: LL991109751021.094, p. 32). Replicate measurements are represented by each data point.

Figure 23. Mean Diameter of Waste Form Colloids Generated from the Corrosion of the SRL 131A Glass in EJ-13 at 2,000/m (T = 90°C) as a Function of Test Duration



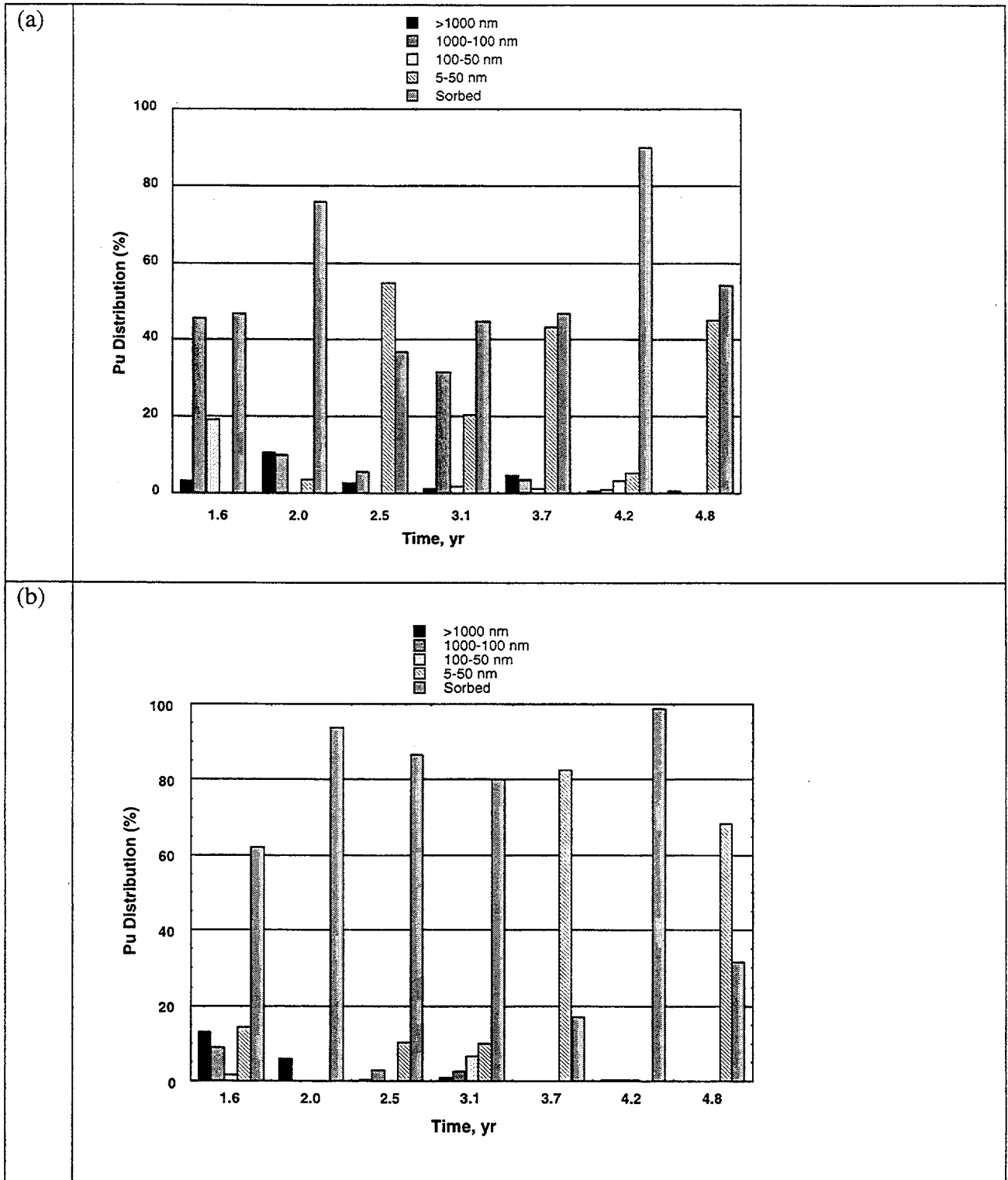
NOTE: Plutonium concentration associated with colloids fraction (450 to 6 nm size fraction from filtration data; DTN: LL000122051021.116) and total colloid concentration (from DLS measurements; DTN: LL991109751021.094, p. 33) as a function of test duration for the SRL 131A glass at 2,000/m (T = 90°C)

Figure 24. Concentration of Pu Colloids and Total Colloid Concentration as a Function of Test Duration for the SRL 131A Glass at 2,000/m (T = 90°C)

6.3.2 Size Distribution of Colloids Generated from Spent Fuel Corrosion

In Figure 25, the distribution of Pu associated with various size fractions in the leachate from the high-drip-rate tests of the ATM-103 and ATM-106 is presented (DTN: LL991001251021.090, Figs. 15 and 16). Sequential filtration data is not available prior to 1.6 years, since the filtration technique was first initiated on the leachates from the 1.6-year test interval. As seen in Figure 25, the Pu is primarily sorbed on the vessel wall for the high-drip-rate tests on both fuels (except for the 3.7- and 4.8-year test interval of the ATM-106 where the 5 - 50 nm fraction is the dominant form of Pu). A significant fraction of filterable Pu was detected from most filtrates in the ATM-103 tests. The dissolved fraction (not presented in Fig. 25 for the Pu distribution) was below detection limits in the leachates for both fuels for test intervals between 1.6 and 4.8 years, except for the ATM-103 high-drip-rate test at the 1.6-year test interval:

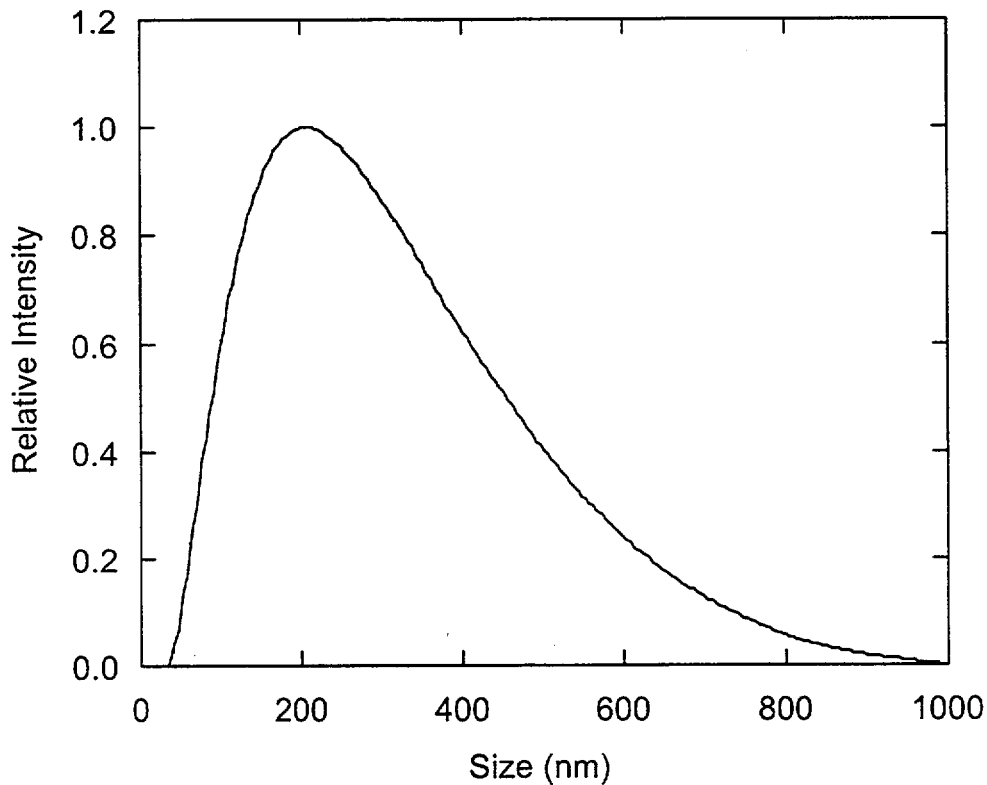
$$([\text{Pu}]_{\text{nonfilterable}} = 4 \times 10^{-10} \text{ M}).$$



NOTE: The Pu distribution in the leachate as a function of time from high-drip-rate tests on the (a) ATM-103 and (b) ATM-106 fuels (DTN: LL991001251021.090, Figs. 15 and 16)

Figure 25. The Pu Distribution in the Leachate as a Function of Time from High-Drip-Rate Tests on the ATM-103 and ATM-106 Fuels

Unsaturated tests with ATM-103 (burnup of ~30 MWd/kgU) and ATM-106 (burnup of ~45 MWd/kgU) fuel were sampled at 56 and 62 months and unfiltered aliquots were taken for DLS measurements. The tests were designed to replicate the interactions at 90°C between spent fuel and EJ-13 groundwater either as water vapor or as small amounts of dripping water (low drip tests, 0.075 mL/3.5 d or high drip tests, 0.75 mL/3.5 d). Dynamic light scattering measurements on only one of the twelve samples indicated the presence of colloids above the detection limits of the system (DTN: LL991109851021.095, pp. 83-85, 89-90, 142-145, 172-173; DTN: LL991109751021.094, p. 34). The leachate from the 56-month sampling of the vapor test with ATM-106 was examined with DLS at 20 mW and at various sample times. Cumulants analysis of the DLS data indicated a wide particle distribution, which was resolved with Contin (Refer to Sec. 6.3). Although the signal was noisy and the count rate was slightly above background levels, the DLS analysis was able to resolve colloidal particulate with a mean diameter of 300 nm at a concentration of 30 ppb. The monomodal distribution obtained from Contin is shown in Figure 26.



NOTE: Contin analysis (see Sec. 6.3) was used to fit the DLS intensity autocorrelation function (DTN: LL991109751021.094, p. 34).

Figure 26. Particle Distribution for Colloids in Leachate from 56 Month ATM-106 Vapor Test

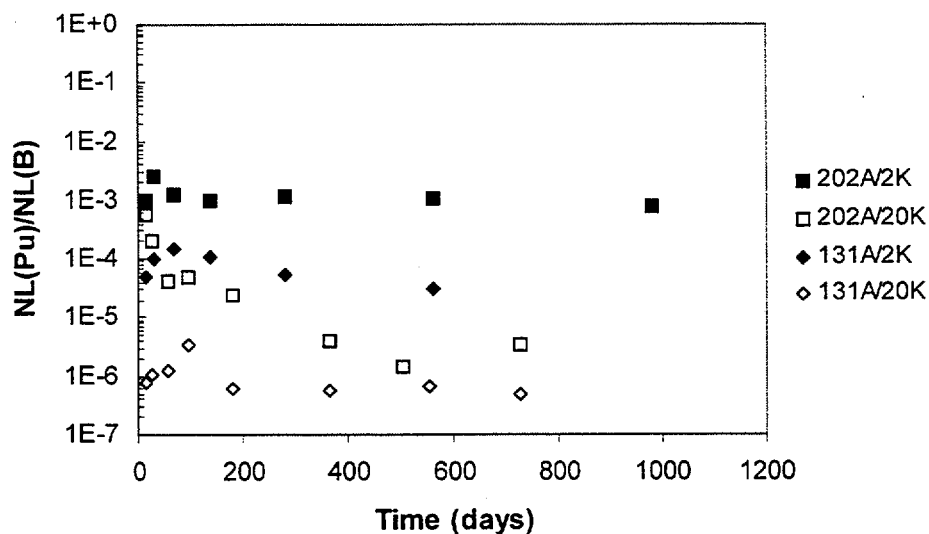
6.4 QUANTIFICATION OF WASTE FORM COLLOIDS

The analyses presented in this section summarize the quantification of colloids generated during the corrosion of defense high level waste glass and commercial spent nuclear fuel. Data used in these analyses include normalized mass loss (NL) data on the corrosion of the waste form and normalized rate (NR) of formation of Pu-associated with colloids. The data encompasses several years of testing for the static glass tests (Ebert 1995), over ten years of testing for the glass drip tests (Fortner and Bates 1996; Fortner et al. 1997a, 1997b; DTN: LL000205551021.118), and testing data from 1.6 to 4.8 years of spent fuel tests (Finn et al. 1994a, 1994b; DTN: LL991001251021.090). The methods employed for colloid quantification in this section are filtration (analysis of filtrates with ICP-MS or alpha spectroscopy). Analysis of the leachate compositions was performed with ICP-MS. In summary, the rate of formation of colloids from waste form corrosion are correlated with the extent of waste form corrosion.

6.4.1 Quantification of Colloids Generated from Glass Tests

An analysis of the quantity of waste form colloids generated from glass corrosion is described in this section. This approach involves the use of experimental data on the corrosion of the waste form and colloid generation to derive an expression for the rate of colloid formation.

The normalized mass loss (NL) of B is available in DTN: LL000123351021.117; the average of duplicate tests were taken when available. The NL(Pu) were calculated from $NL_i \text{ (g/m}^2\text{)} = (i \text{ in ng}) / \{[(\text{volume in mL}) * (\text{g}/10^9\text{ng}) * (10^6 \text{ cm}^3/\text{m}^3)] / (\text{S/V in m}^{-1}) / (f_i)\}$, where the surface area to volume ratio is S/V and the weight fraction (f_i) of Pu is 0.01 in the SRL 202A and SRL 131A glasses. When the normalized mass loss of Pu, NL(Pu), is compared to the normalized mass loss of boron, NL(B), for the corrosion of a glass, the ratio indicates the amount of Pu released relative to the amount of glass corroded. A ratio of one indicates congruent release of both components. As seen in Figure 27, the NL(Pu) is consistently lower than the NL(B) by at least two orders of magnitude for the SRL 202A glass reacted at 2,000 and 20,000/m, but the NL(Pu)/NL(B) decreases sharply at longer test durations at 20,000/m. The NL(Pu) is at least three orders of magnitude lower than NL(B) for the corrosion of the SRL 131A glass. The decrease in NL(Pu)/NL(B) at ~100 days for the corrosion of the SRL 202A glass at 20,000/m and after 280 days for the corrosion of the 131A glass at 2,000/m corresponds to an increase in the glass corrosion rate due to secondary phase formation and destabilization of the colloids. The NL(Pu) is more than four orders of magnitude lower than the NL(B) when the solution conditions inhibit stable colloids.



NOTE: Ratio of normalized mass loss of plutonium to normalized mass loss of boron, NL(Pu)/NL(B), as a function of test duration (in days) for static corrosion tests on the SRL 202A and SRL 131A glasses at 2,000 and 20,000/m ($T = 90^{\circ}\text{C}$) (DTN: LL000122051021.116 for the Pu data and DTN: LL000123351021.117 for the B data).

Figure 27. Ratio of Normalized Mass Loss of Plutonium to Normalized Mass Loss of Boron as a Function of Test Duration (in days) for Static Corrosion Tests on the SRL 202A and SRL 131A Glasses

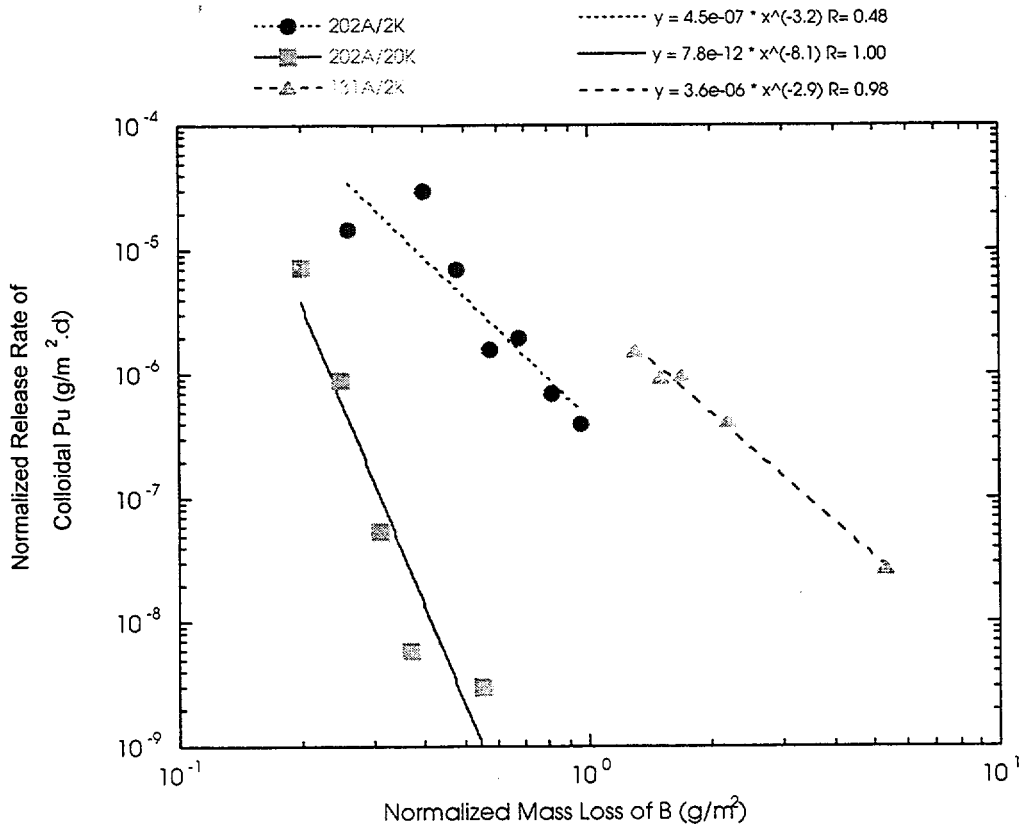
6.4.2 Recommendations for Modeling Colloid Generation

During early reaction of waste glass under unsaturated drip test conditions and static test conditions, the glass dissolves and releases glass components at a rate proportional to the corrosion of the waste form. Boron is used as a marker of the extent of glass corrosion since it is a highly soluble glass component, and it does not get incorporated into alteration phases. As the glass dissolves, dissolution of the waste form results in solution conditions that promote nucleation of clay colloids and the formation of clay alteration layers on the surface of the glass. These clay phases sorb ionic actinide species or colloidal actinide-bearing phases. Under low ionic strength solution conditions, the colloids are stable in solution and the rate of formation of Pu-bearing colloids ($dm_{\text{Pu-coll}}/dt$) is proportional to the amount of altered glass (M_{alt}). Experimental data from the static corrosion of two waste glasses (at two surface area of glass-to-volume ratios) show that the rate of Pu-bearing colloid formation decreases as the glass alters (Fig. 28). This behavior is also observed in the glass drip tests (Fig. 29). The initial response is a power-law decrease in Pu rate with glass corrosion, which can be attributed to sorption by a fixed clay alteration layer. The rate of Pu-colloid formation can be described by a power law relationship, as shown in Equation 1:

$$\frac{dm_{\text{Pu-coll}}}{dt} = a(M_{\text{alt}})^{-b} \quad (\text{Eq. 1})$$

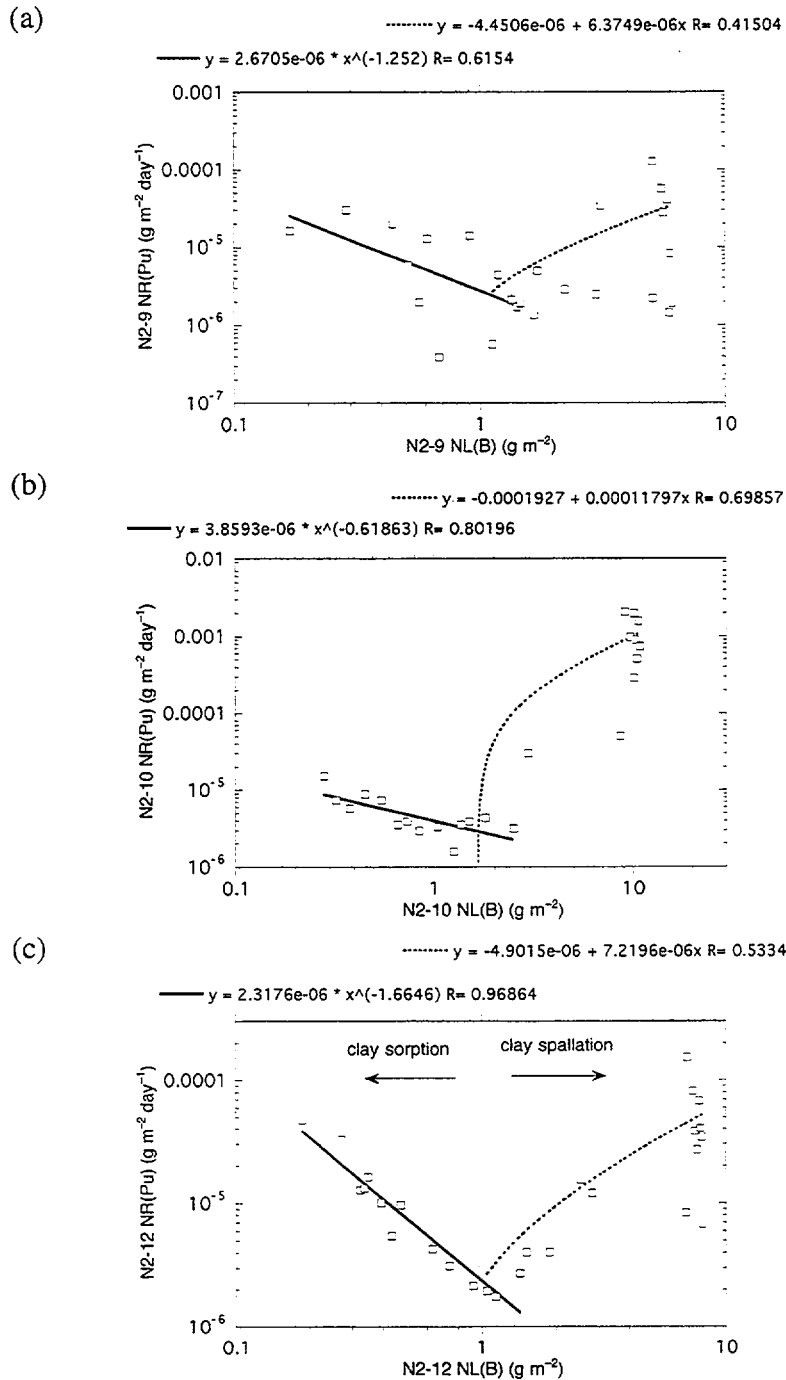
Variations in the constants, a and b , obtained for the various glasses may be a function of the surface area-to-volume ratio, leachate composition (ionic strength, etc.), colloid composition, or other experimental parameters. The experimental range of a values is 4×10^{-6} to 8×10^{-12} (for the static glass tests, Fig. 28) and 2×10^{-6} to 5×10^{-6} (for the glass drip tests, Fig. 29). The

experimental range of b values is 3 to 8 (for the static tests, Fig. 28), and 0.3 to 1.7 (for the glass drip tests, Fig. 29). Bounding values based upon the experimental data are 0.0001 days^{-1} for a and 1 for b . The correlation between the rate of colloid formation and the alteration of the glass suggests that the mechanism for colloid formation is related to the accumulated mass of alteration products.



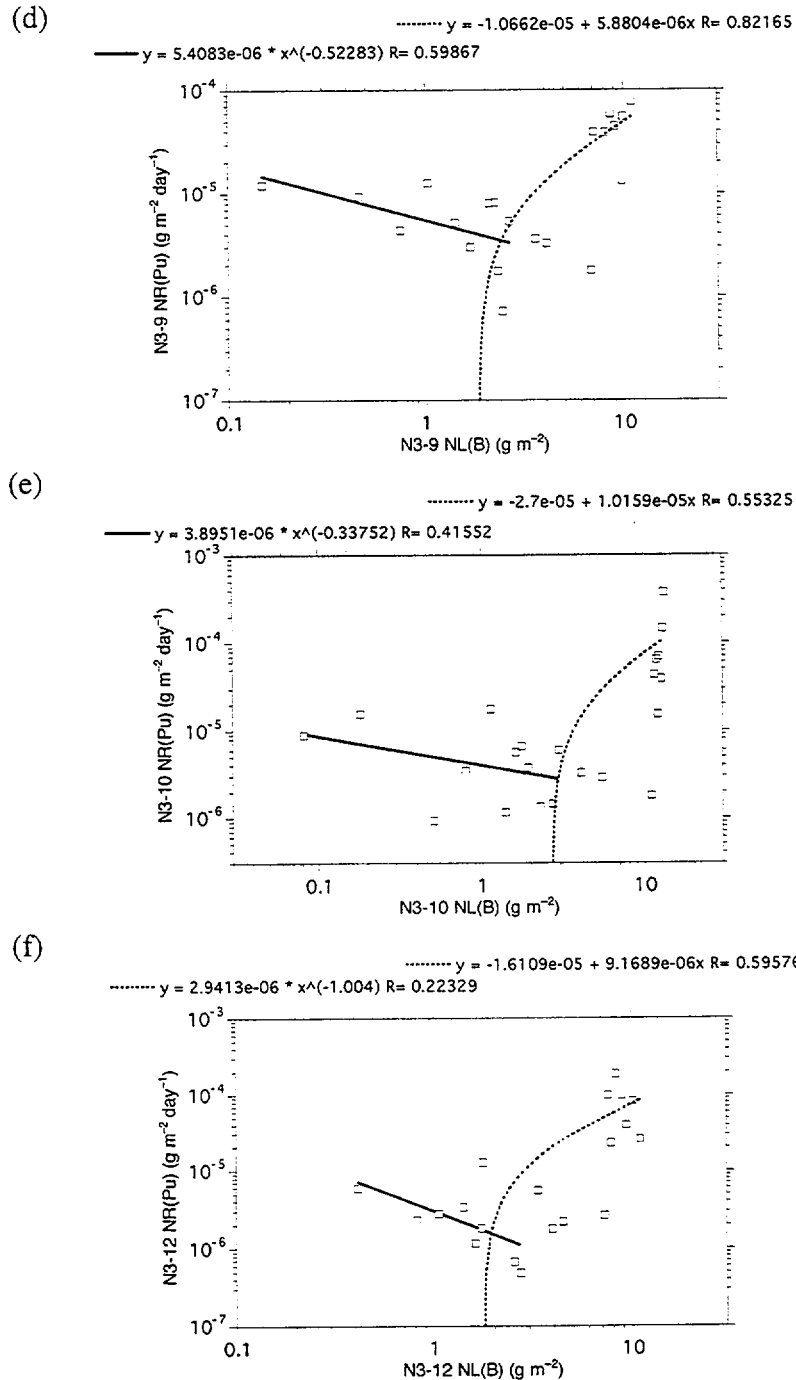
NOTE: Data for colloidal Pu from LL0001 and data for boron from LL0001, Appendix D.3, pp. 214, 220, 227; DTN: LL991109751021.094 (p. 36)

Figure 28. Normalized Release Rate of Colloidal Plutonium as a Function of Normalized Mass Loss of Boron for SRL 202A and SRL 131A Glasses at 2,000 and 20,000/m



NOTE: Plutonium release rate (calculated for each sampling interval) versus cumulative boron release: (a) N2-9, (b) N2-10, and (c) N2-12. The total plutonium release is used, including vessel acid strip. Data extracted from DTN: LL000205551021.118. Data analysis from DTN: LL991110551021.102, pp. 44-49.

Figure 29. Plutonium Release Rate versus Cumulative Boron Release for N2 and N3 Glass-Drip Tests



NOTE: Plutonium release rate (calculated for each sampling interval) versus cumulative boron release: (d) N3-9, (e) N3-10, and (f) N3-12. The total plutonium release is used, including vessel acid strip. Data extracted from DTN: LL000205551021.118. Data analysis from DTN: LL991110551021.102 pp. 44-49.

Figure 29. Plutonium Release Rate versus Cumulative Boron Release for N2 and N3 Glass-Drip Tests (continued)

In the high ionic strength regime for the static glass corrosion test conditions, the concentration of Pu-colloids was insufficient to derive a correlation between the formation rate of Pu-colloids and the corrosion of the altered glass (refer to Fig. 8 for Pu-colloids as a function of ionic

strength). The amount of colloids present in high ionic strength solutions was very low since the clay colloids were destabilized. In the glass drip tests, the ionic strength remains low due to the injected EJ-13 water. However, another mechanism of colloid formation is evident in the unsaturated drip tests at long test durations where the spallation of Pu-bearing colloids dominates the long-term release of plutonium from the waste form. Once the cumulative boron release is greater than $\sim 1\text{-}3 \text{ g m}^{-2}$, the release of plutonium is controlled by spallation of this layer and, thereby, to the total amount of glass reacted (DTN: LL000205551021.118). Owing to the stochastic nature of colloid spalling, the scatter in the data is large. Nonetheless, the relationship is consistent with a plutonium release rate depending upon total amount of glass corrosion.

An analysis of the test results and the known reaction mechanisms leads us to propose a two-step process for generating colloids from the waste form. The first step is the corrosive alteration of the emplaced waste form. The second step is the erosion of colloidal particulates from the compromised material generated by the corrosion. Thus, the release of plutonium colloids is proportional to the amount of *altered* waste form available to release colloidal material. The first step in this process can be represented by the following equation:

Step 1

$$M_{alt} = A \cdot \int_0^t (NR_i(\tau) - NR_{Pu}(\tau)) d\tau \quad (\text{Eq. 2})$$

where M_{alt} is the mass of altered waste form that contains plutonium, A is the surface area, t is the elapsed time, and $NR_i(t)$ is the normalized release rate of marker element i (B for glass). Note the correction for NR_{Pu} , the total normalized release rate of Pu; this term is negligible over the time scale of our laboratory experiments where NR_B exceeds NR_{Pu} by several orders of magnitude. This correction appears for physical reasons (to conserve mass) and becomes significant at long times when a large fraction of the waste form has been altered. Note also that Equation 1 considers only waste form colloids. Consider the example of corrosion by congruent dissolution, where $NL_i = NL_{Pu}$ for all i , and the integrand vanishes. In such a case the colloids, if present, must be pseudocolloids or radiocolloids, which form by different processes independent of the waste form.

The release of spallation colloids is represented by:

Step 2

$$\frac{dm_{Pu_{coll}}}{dt} = \kappa M_{alt} \quad (\text{Eq. 3})$$

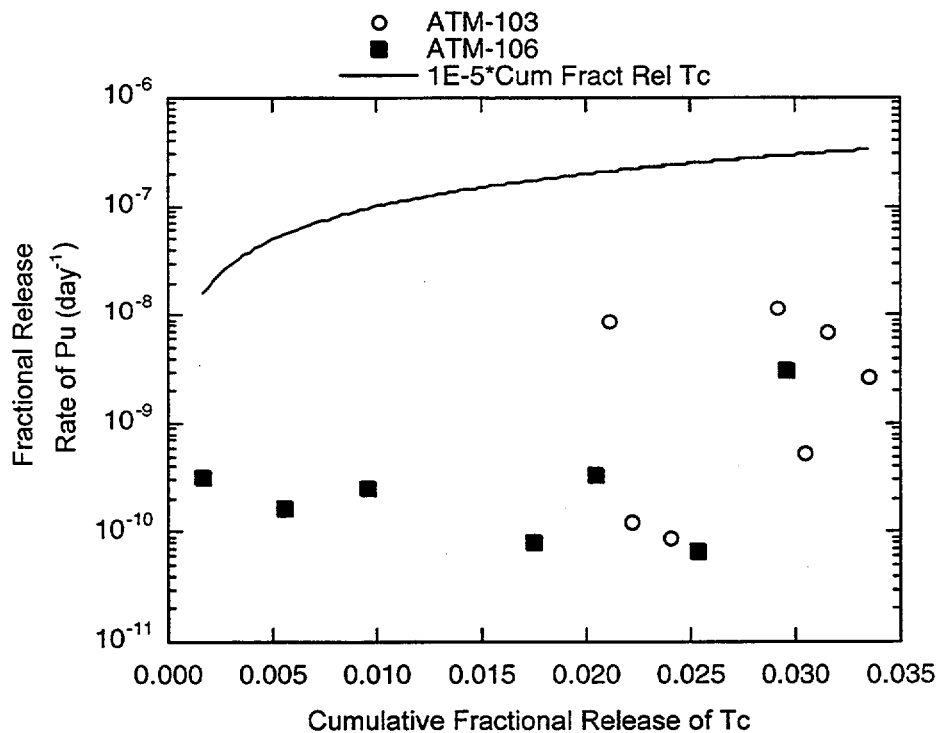
where $m_{Pu_{coll}}$ is the mass release of plutonium suspended as colloidal particulates, and κ is a parameter that will depend on the mechanical condition of the altered waste form and other factors including the flow rate of water over the waste form and the water chemistry. The rate at which these spallation colloids are generated, $\frac{dm_{Pu_{coll}}}{dt}$, is given by Equation 3. We can determine κ for our experimental conditions of static tests or unsaturated drip tests. Based upon Figure 29, an empirical bound for κ is 10^{-4} d^{-1} . The experimental test is to see whether the rate of suspended plutonium release is proportional to the cumulative release of boron. Note that the

above mechanism considers only waste form colloids spalled from the glass; this mechanism does not apply to radiocolloids, which are solubility-controlled.

6.4.3 Quantification of Colloids Generated from Spent Fuel Corrosion

In comparison with the work by Efurud et al. (1998) on the solubility limits of Pu in J-13 water, the concentration of Pu in the SNF test leachates is close to the solubility limits of Pu in J-13 at 25°C. At each sampling interval, the Pu concentration in the SNF tests was between 10^{-10} and 10^{-8} M; whereas, solubility limits in J-13 were determined to be $4.7 \pm 1.1 \times 10^{-8}$, $2.4 \pm 1.2 \times 10^{-8}$, and $9.4 \pm 1.6 \times 10^{-8}$, at pH 6, 7, and 8.5 respectively at 25°C. The Pu solubilities at 90°C were ten times lower than the solubilities at 25°C.

The reaction of spent nuclear fuel under unsaturated drip test conditions does not exhibit a correlation between the rate of Pu-bearing colloid formation and the corrosion of the spent fuel. Figure 30 represents the fractional release rate of Pu as a function of cumulative fractional release of Tc for the ATM-103 and ATM-106 high-drip-rate tests (DTN: LL991109751021.094, p. 37). Technetium is used as a marker of the extent of spent fuel corrosion. Technetium is a soluble element, which is released from the fuel to a greater extent than other elements, such as Cs and Sr (these are incorporated in alteration phases). Since the fractional release rate of Pu and the cumulative fractional release of Tc are proportional respectively to the NR(Pu) and NL(Tc), an empirical bounding estimate of the normalized rate of Pu-bearing colloid formation is 10^{-5} times the normalized loss of Tc per day.



NOTE: DTN: LL991109751021.094 (p. 37). The solid line is the conservative bound based upon a constant of 10^{-5} d^{-1} .

Figure 30. The Fractional Release Rate of Pu as a Function of Cumulative Fractional Tc Release for the ATM-103 and ATM-106 High-Drip-Rate Tests

After the simulated groundwater solution passed through the fuel assembly, the reported pH at 25°C was lowered to between 4.5 and 6.2. This may be a consequence of the radiolysis (Finn et al. 1994a); however, the precipitation of some uranyl alteration phases may also lower the pH. Generally, the formation of Pu hydrolysis colloids increases with increasing pH. Conditions in these spent fuel tests would have been unfavorable for the formation of Pu-polymer colloids (real colloids).

Plutonium and americium have not been detected in uranyl alteration phases but seem to remain in residues on the surface of the corroding fuel. Evidence from the leachates supports the contention that the majority of the plutonium has not been released (DTN: LL991001251021.090). The occurrence of the plutonium-rich residues that are believed to be formed during the corrosion of spent fuel under laboratory testing conditions explains the low concentration of Pu in the leachates (DTN: LL991110351021.100, p. 36).

The main points of this work may be summarized as: (1) the majority of Pu and Am remains at the corroded fuel surface as determined by TEM analyses, (2) Pu, Am, and Cm are present as filterable material in the leachate at pH values of 6 to 8, (3) the Pu colloidal concentrations are similar to Pu solubility limits reported in J-13 water by Efurud et al. (1998), and (4) the normalized filterable Pu release rate (per day) is at least five orders of magnitude lower than the corrosion of the fuel as estimated by NL(Tc). The data from the Commercial Spent Nuclear Fuel (CSNF) tests indicates that Pu is retained in a layer attached to the corroded fuel surface. Within the duration of the CSNF tests at ANL, only a very small fraction of this plutonium has been removed or spalled from the surface (rate $<10^{-5} \text{ d}^{-1}$) (DTN: LL991109751021.094, p. 37).

7. CONCLUSIONS

The conclusions from this analysis are: evidence from static corrosion tests on high-level waste (HLW) glass indicates that the dominant type of colloidal material consists of a smectite clay substrate often incorporating discrete phases within the clay matrix which can contain high concentrations of sparingly soluble radioelements (e.g., Pu).

The experimental evidence indicates that, in the HLW glass tests, the clay colloids can form as a result of homogenous nucleation of clay phases in the leachate and as a result of spallation of clay alteration layers from the corroding glass surface.

The experimental evidence for the glass corrosion tests presented in this analysis indicates that there is a critical ionic strength ($\sim 0.05 \text{ M}$) above which the colloids formed in the glass corrosion tests are unstable; very low colloid concentrations are observed above the critical ionic strength (see Fig. 8).

The available data from dynamic light scattering of the colloids observed in the low ionic strength regime in HLW glass tests show that the colloids have a lognormal size distribution with a mean size of approximately 120-160 nm (see Fig. 23).

The observed correlations for the glass batch and drip test data (see Figs. 28 and 29) provide a basis for empirical estimates of the rate of colloid formation under the test conditions. The data fall into two categories depending on the extent of glass corrosion as indicated by the normalized

loss (or release) or boron NL(B). For low values of NL(B), the NR(Pu_{coll}) (i.e., the normalized release rate of Pu in colloidal form) is given by the following expression:

$$\text{NR(Pu}_{\text{coll}}) = a [\text{NL(B)}]^{-b}$$

where

a and b = empirically determined constants (see Figs. 28 and 29 for the empirically determined values in units of d⁻¹).

For higher values of NL(B) i.e., when the corrosion of the glass has progressed to a greater extent, the NR(Pu_{coll}) is given by the following expression (spallation becomes the dominant mechanism):

$$\text{NR(Pu}_{\text{coll}}) = \kappa [\text{NL(B)}]$$

where

κ = empirically-determined constant (see Fig. 29 for the empirically-determined values in units of d⁻¹).

The generation of colloids in this case is governed by the spallation of colloidal sized plutonium bearing particles. Because the former expression is a decreasing function, the rate of waste glass colloid generation is dominated by the latter contribution as the extent of corrosion progresses.

The spent fuel drip test data (see Fig. 30) provide an initial basis for bounding estimates of the rate of colloid formation under the test conditions. The normalized release rate of Pu-bearing colloids is less than 10⁻⁵ times the normalized loss of technetium per day.

8. INPUTS AND REFERENCES

8.1 DOCUMENTS CITED

Ahn, T.; Interrante, C.G.; and Weller, R.A. 1993. "A Justification for the Use of Data from Accelerated Leach Tests of Glass." *Materials Research Society Symposium Proceedings*, 294, 599-604. Pittsburgh, Pennsylvania: Materials Research Society. TIC: 208880.

Bates, J.K. and Buck, E.C. 1994a. "Results of Drip Tests on Sludge-Based and Actinide-Doped Glasses." *High Level Radioactive Waste Management, Proceedings of the Fifth Annual International Conference, Las Vegas, Nevada, May 22-26, 1994*, 2, 1088-1101. La Grange Park, Illinois: American Nuclear Society. TIC: 210984.

Bates, J.K. and Buck, E.C. 1994b. "Waste Glass Weathering." *Scientific Basis for Nuclear Waste Management XVII, Symposium held November 29-December 3, 1993, Boston, Massachusetts*. Barkatt, A. and Van Konynenburg, R.A., eds. 333, 41-53. Pittsburgh, Pennsylvania: Materials Research Society. TIC: 213541.

Bates, J.K.; Bourcier, W.L.; Bradley, C.R.; Buck, E.C.; Cunnane, J.C.; Dietz, N.L.; Ebert, W.L.; Emery, J.W.; Ewing, R.C.; Feng, X.; Gerding, T.J.; Gong, M.; Hoh, J.C.; Li, H.; Mazer, J.J.; Morgan, L.E.; Newton, L.; Nielsen, J.K.; Phillips, B.L.; Tomozawa, M.; Wang, L.; and Wronkiewicz, D.J. 1993. *ANL Technical Support Program for DOE Environmental Restoration and Waste Management. Annual Report, October 1991-September 1992*. ANL-93/13. Argonne, Illinois: Argonne National Laboratory. TIC: 244798.

Bates, J.K.; Bourcier, W.L.; Bradley, C.R.; Brown, N.R.; Buck, E.C.; Carroll, S.A.; Cunnane, J.C.; Dietz, N.L.; DiSanto, T.; Ebert, W.L.; Emery, J.W.; Feng, X.; Gerding, T.J.; Gong, M.; Hafenrichter, L.D.; Hoh, J.C.; Mazer, J.J.; Newton, L.; Phillips, B.L.; Pletcher, R.; and Wronkiewicz, D.J. 1994. *ANL Technical Support Program for DOE Environmental Restoration and Waste Management. Annual Report, October 1992-September 1993*. ANL-94/19. Argonne, Illinois: Argonne National Laboratory. TIC: 219202.

Bates, J.K.; Buck, E.C.; Dietz, N.L.; DiSanto, T.; Ebert, W.L.; Emery, J.W.; Fortner, J.A.; Hafenrichter, L.D.; Hoh, J.C.; Luo, J.S.; Nunez, L.; Surchik, M.T.; Wolf, S.F.; and Wronkiewicz, D.J. 1996. *ANL Technical Support Program for DOE Office of Environmental Management. Annual Report, October 1994--September 1995*. ANL-96/11. Argonne, Illinois: Argonne National Laboratory. TIC: 246107.

Buck, E.C. and Bates, J.K. 1999. "Microanalysis of Colloids and Suspended Particles from Nuclear Waste Glass Alteration." *Applied Geochemistry*, 14, 635-653. New York, New York: Elsevier Science Ltd. TIC: 245946.

Buck, E.C. and Fortner, J.A. 1997. "Detecting Low Levels of Transuranics with Electron Energy Loss Spectroscopy." *Ultramicroscopy*, 67, 69-75. Amsterdam, The Netherlands: Elsevier Science. TIC: 246495.

Buck, E.C.; Bates, J.K.; and Feng, X. 1994. "Colloid Formation During the Corrosion of SRL 200 Glass." *Environmental and Waste Management Issues in the Ceramic Industry II, Symposium held April 25-27, 1994, Indianapolis, Indiana*. Bickford, D., Bates, S., Jain, V., Smith, G., eds. Ceramic Transactions, 45. p. 187-197. Westerville, Ohio: American Ceramic Society. TIC: 246319.

Buck, E.C.; Bates, J.K.; Cunnane, J.C.; Ebert, W.L.; Feng, X.; and Wronkiewicz, D.J. 1993. "Analytical Electron Microscopy Study of Colloids from Nuclear Waste Glass Reaction." *Materials Research Society Symposium Proceedings*. 294, 199-206. Pittsburgh, Pennsylvania: Materials Research Society. TIC: 208880.

CRWMS M&O 1999a. *Classification of the MGR Uncanistered Spent Nuclear Fuel Disposal Container System*. ANL-UDC-SE-000001 REV 00. Las Vegas, Nevada: CRWMS M&O. ACC: MOL.19990928.0216.

CRWMS M&O 1999b. *Activity Evaluation for 1101213FM3 Waste Form Analyses & Models - PMR*. Activity Evaluation, December 14, 1999. Las Vegas, NV: CRWMS M&O. ACC: MOL.19991217.0048.

CRWMS M&O 2000. *Waste Package Materials Department Analysis and Modeling Reports Supporting the Waste Form PMR*. TDP-EBS-MD-000005 REV 01 . Las Vegas, Nevada: CRWMS M&O. ACC: MOL.20000202.0173.

Cunnane, J.C. and Bates, J.K. 1991. "Identification of Colloids in Nuclear Waste Glass Reactions." *Ceramic Transactions, Nuclear Waste Management IV*. Wicks, G.C.; Bickford, D.F.; and Bunnell, L.R. eds. 65-73. Westerville, Ohio: The American Ceramic Society. TIC: 221716.

Curti, E.; Godon, N.; and Vernaz, E.Y. 1993. "Enhancement of the Glass Corrosion in the Presence of Clay Minerals: Testing Experimental Results with an Integrated Glass Dissolution Model." *Scientific Basis for Nuclear Waste Management XVI, Symposium held November 30-December 4, 1992, Boston, Massachusetts*. Interrante, C.G. and Pabalan, R.T., eds. 294, p. 163-170. Pittsburgh, Pennsylvania: Materials Research Society. TIC: 208880.

Degueldre, C.; Scholtis, A.; Pearson, F.J.; Laube, A.; and Gomez, P. 1999. "Effect of Sampling Conditions on Colloids and Ground Water Chemistry." *Eclogae Geologicae Helvetiae*, 92, 105-114. Basel, Switzerland: Birkhauser Verlag . TIC: 246635.

DOE (U.S. Department of Energy) 2000. *Quality Assurance Requirements and Description*. DOE/RW-0333P, Rev. 9. Washington, D.C.: U.S. Department of Energy, Office of Civilian Radioactive Waste Management. ACC: MOL.19991028.0012.

Ebert, W.L. 1995. *The Effects of the Glass Surface Area/Solution Volume Ratio on Glass Corrosion: A Critical Review*. ANL-94/34. Argonne, Illinois: Argonne National Laboratory. TIC: 215400.

Ebert, W. and Bates, J.K. 1993. "A Comparison of Glass Reaction at High and Low Glass Surface/Solution Volume." *Nuclear Technology*, 104, 372-384. Hinsdale, Illinois: American Nuclear Society. TIC: 246461.

Efurd, D.W.; Runde, W.; Banar, J.C.; Janecky, D.R.; Kaszuba, J.P.; Palmer, P.D.; Roensch, F.R.; and Tait, D. 1998. "Neptunium and Plutonium Solubilities in a Yucca Mountain Groundwater." *Environmental Science & Technology*, 32, (24), 3893-3900. Easton, Pennsylvania: Environmental Science & Technology. TIC: 243857.

Feng, X.; Buck, E.C.; Mertz, C.; Bates, J.K.; Cunnane, J.C.; and Chaiko, D.J. 1994. "Characteristics of Colloids Generated during the Corrosion of Nuclear Waste Glasses in Groundwater." *Radiochimica Acta*, 66/67, 197-205. Munchen, Germany: R. Oldenbourg Verlag. TIC: 238720.

Finn, P.A.; Buck, E.C.; Gong, M.; Hoh, J.C.; Emery, J.W.; Hafenrichter, L.D.; and Bates, J.K. 1994a. "Colloidal Products and Actinide Species in Leachate from Spent Nuclear Fuel." *Radiochimica Acta*, 66/67, 197-203. Munchen, Germany: R. Oldenbourg Verlag. TIC: 238493.

Finn, P.A.; Hoh, J.C.; Bates, J.K.; and Wolf, S.F. 1994b. "Behavior of Spent Fuel Under Unsaturated Conditions." *Proceedings of the Topical Meeting on DOE Spent Nuclear Fuel—Challenges and Initiatives, Salt Lake City, Utah, December 13-16, 1994*. Pages 421-429. La Grange Park, Illinois: American Nuclear Society. TIC: 103316.

Fortner, J.A. and Bates, J.K. 1996. "Long-Term Results from Unsaturated Durability Testing of Actinide-Doped DWPF and WVDP Waste Glasses." *Scientific Basis for Nuclear Waste Management XIX, Symposium held November 27-December 1, 1995, Boston, Massachusetts*. Murphy, W.M. and Knecht, D.A., eds. 412, 205-211. Pittsburgh, Pennsylvania: Materials Research Society. TIC: 233877.

Fortner, J.A.; Bates, J.K.; and Gerding, T.J. 1997a. *Analysis of Components from Drip Tests with ATM-10 Glass*. ANL-96/16. Argonne, Illinois: Argonne National Laboratory. TIC: 246306.

Fortner, J.A.; Gerding, T.J.; and Bates, J.K. 1995. "Long-Term Test Results from a West Valley Actinide-Doped Reference Glass." *Proceedings of the International Symposium on Environmental Issues and Waste Management Technologies in the Ceramic and Nuclear Industries, presented at the 97th Annual Meeting of the American Ceramic Society, held in Cincinnati, May 1 - 3, 1995*. 61, 455 - 462. Westerville, Ohio: American Ceramic Society. TIC: 246649.

Fortner, J.A.; Wolf, S.F.; Buck, E.C.; Mertz, C.J.; and Bates, J.K. 1997b. "Solution-Borne Colloids from Drip Tests Using Actinide-Doped and Fully-Radioactive Waste Glasses." *Materials Research Society Symposium Proceedings*. 465, 165-172. Pittsburgh, Pennsylvania: Materials Research Society. TIC: 238884.

Geckeis, H.; Grambow, B.; Loida, A.; Luckscheiter, B.; Smailos, E.; and Quinones, J. 1998. "Formation and Stability of Colloids Under Simulated Near Field Conditions." *Radiochimica Acta*, 82, 123-128. Munchen, Germany: R. Oldenbourg Verlag. TIC: 246443.

Johnsen, R.M. and Brown, W. 1992. "An Overview of Current Methods of Analyzing QLS Data." Chapter 6 of *Laser Light Scattering in Biochemistry*. Harding, S.E.; Sattelle, D.B. and

Bloomfield, V.A., eds. Cambridge, United Kingdom: The Royal Society of Chemistry. TIC: 246586.

Kersting, A.B.; Efurud, D.W.; Finnegan, D.L.; Rokop, D.J.; Smith, D.K.; and Thompson, J.L. 1999. "Migration of Plutonium in Ground Water at the Nevada Test Site." *Nature*, 397, 56-59. London, England: Macmillan Publishers. TIC: 243597.

Kim, J.I. 1994. "Actinide Colloids in Natural Aquifer Systems." *MRS Bulletin*, 19, (12), 47-53. Pittsburgh, Pennsylvania: Materials Research Society. TIC: 246128.

McCarthy, J.F. and Degueldre, C. 1993. "Sampling and Characterization of Colloids and Particles in Groundwater for Studying Their Role in Contaminant Transport." Chapter 6 of *Environmental Particles*. Buffle, J. and van Leeuwen, H.P., eds. Volume 2. Boca Raton, Florida: Lewis Publishers. TIC: 245905.

Olofsson, U.; Allard, B.; Andersson, K.; and Torstenfelt, B. 1982. "Formation and Properties of Americium Colloids in Aqueous Systems." *The Scientific Basis for Nuclear Waste Management. II*, 191-198. New York, New York: Elsevier Science Publishing Company. TIC: 204398.

Schurtenberger, P. and Newman, M.E. 1993. "Characterization of Biological and Environmental Particles Using Static and Dynamic Light Scattering." Chapter 2 of *Environmental Particles*. Buffle, J. and van Leeuwen, H.P. eds. Volume 2. Boca Raton, Florida: Lewis Publishers. TIC: 247010.

Thomas, L.E.; Beyer, C.E.; and Charlot, L.A. 1992. "Microstructural Analysis of LWR Spent Fuels at High Burnup." *Journal of Nuclear Materials*, 188, 80-89. Amsterdam, The Netherlands: Elsevier Science Publishers. TIC: 235249.

van Olphen, H. 1977. *An Introduction to Clay Colloid Chemistry for Clay Technologists, Geologists, and Soil Scientists*. 2nd Edition. New York, New York: John Wiley & Sons. TIC: 208918.

Wronkiewicz, D.J.; Bates, J.K.; Wolf, S.F.; and Buck, E.C. 1996. "Ten-Year Results from Unsaturated Drip Tests with UO₂ at 90°C: Implications for the Corrosion of Spent Nuclear Fuel." *Journal of Nuclear Materials*, 238, (1), 78-95. Amsterdam, The Netherlands: North-Holland Publishing Company. TIC: 243361.

8.2 CODES, STANDARDS, REGULATIONS, AND PROCEDURES

AP-3.10Q, Rev. 2, ICN 0. *Analyses and Models*. Washington, D.C.: U.S. Department of Energy, Office of Civilian Radioactive Waste Management. ACC: MOL.20000217.0246.

ASTM C 1174-97. 1997. *Standard Practice for Prediction of the Long-Term Behavior of Materials, Including Waste Forms, Used in Engineered Barrier Systems (EBS) for Geological Disposal of High-Level Radioactive Waste*. West Conshohocken, Pennsylvania: American Society for Testing and Materials. TIC: 246015.

QAP-2-3, Rev. 10. *Classification of Permanent Items*. Las Vegas, Nevada: CRWMS M&O. ACC: MOL.19990316.0006.

QAP-2-0, Rev. 5, ICN 1. *Conduct of Activities*. Las Vegas, Nevada: CRWMS M&O. ACC: MOL.19991109.0221.

8.3 SOURCE DATA

LL991001251021.090. Draft - CSNF Waste Form Degradation: Unsaturated Drip Tests - G2020 Analysis and Modeling Report . Submittal date: 10/04/1999.

LL991109751021.094. Data Associated with the Detection and Measurement of Colloids In Scientific Notebook SN 1644. Submittal date: 01/10/2000.

LL991109851021.095. Colloid Size and Concentration Investigations in Scientific Notebook SN 1381. Submittal date: 01/10/2000.

LL991109951021.096. Colloid Detection and Size Determination Investigations in Scientific Notebook SN 1268. Submittal date: 01/10/2000.

LL991110051021.097. Colloid and Clay Concentration Measurements in Scientific Notebook SN 1186. Submittal date: 01/10/2000.

LL991110251021.099. Colloid and Size Concentrations Recorded in Scientific Notebook SN 867. Submittal date: 01/10/2000.

LL991110351021.100. Colloid Size and Concentrations Recorded in Scientific Notebook SN 1528. Submittal date: 01/10/2000.

LL991110451021.101. Colloid and Clay Analysis in Scientific Notebook SN 1355. Submittal date: 01/10/2000.

LL991110551021.102. Plutonium and Boron Release Rates in Scientific Notebook SN 674. Submittal date: 01/10/2000.

LL991110651021.103. Clay and Glass Distributions Recorded in Scientific Notebook SN 1116. . Submittal date: 01/10/2000.

LL991110751021.104. AEM Microscopy of Colloids in Scientific Notebook SN 428. Submittal date: 01/10/2000.

LL991110851021.105. Colloid and Size Concentrations in Scientific Notebook SN 941. Submittal date: 01/10/2000.

LL000122051021.116. Summary of Analyses of Glass Dissolution Filtrates. Submittal date: 01/27/2000.

LL000123351021.117. ANL 94/34 - The Effects of The Glass Surface Area/Solution Volume Ratio on Glass Corrosion: a Critical Review. Submittal date: 01/28/2000.

LL000205551021.118. Solution and Alteration Phase Data for Unsaturated Corrosion Testing of Glass Waste Forms. Submittal date: 02/17/2000.